KR-F LASER SURFACE TREATMENT OF POLY(METHYL METHACRYLATE, GLYCOL-MODIFIED POLY(ETHYLENE TEREPHTHALATE) , AND POLYTETRAFLUOROETHYLENE FOR ENHANCED ADHESION OF *ESCHERICHIA COLI* K-12

Allison Suggs

Thesis submitted to the faculty of Virginia Polytechnic Institute and State University for the partial fulfillment for the degree of

Master of Science

In

Materials Science and Engineering

Approved:

_____

Dr. Brian Love, Chair

_____ _____

Dr. Dwight Viehland Dr. Carlos Suchicital

September 13, 2002

Blacksburg, VA

Keywords: polymer, laser ablation, surface treatment, cellular adhesion

KR-F LASER SURFACE TREATMENT OF POLY(METHYL METHACRYLATE, GLYCOL-MODIFIED POLY(ETHYLENE TEREPHTHALATE) , AND POLYTETRAFLUOROETHYLENE FOR ENHANCED ADHESION OF *ESCHERICHIA COLI* K-12

Allison E. Suggs

(Abstract)

Environmental response as determined by the cell-polymer interaction stands as the greatest restriction to the implementation of new polymeric materials. Cell-polymer interactions are most influenced by the substrate surface free energy, surface chemistry, topography, and rigidity [1]. Alteration of these properties through surface treatment has become a common approach to attain the desired cellular interaction.

This study investigates Kr-F excimer laser (248 nm) surface modification of polymethyl methacrylate (PMMA), glycol-modified polyethylene terephthalate (PETG), and polytetrafluoroethylene (PTFE) and its effect on the adhesion of *Escherichia coli* K-12 bacteria. These three polymers were chosen for their very different mechanisms of ablation as well as their range of surface free energies and bacterial responses [2-4].

Polymers were ablated using a pulsed Kr-F excimer laser with a dose of 3.3×10^9 W/cm^2 per pulse. This high level of UV radiation was sufficient to cause significant surface damage on both PMMA and PTFE. PETG showed some signs of wavering in the surface and material removal was confirmed through optical microscopy. Due to the extensive damage associated with ablation, a much lower radiation dose was required for contact angle measurements to be taken. For this, a lower-powered, continuous beam Kr-F laser was used. It delivered a dose of 1.27 W/cm^2. Contact angle measurements were then taken which showed dose-dependent surface free energy in all three polymers.

Following ablation, bacterial adhesion to PETG was improved two-fold, while it decreased in both PTFE and PMMA. Surface chemistry analysis supported the idea that ablation occurred through chain scission, since there were no new surface groups created.

There were significant texture modifications observed in PTFE and PMMA while PETG demonstrated the rolling structure characteristic of polyesters following laser ablation described in Wefers et al [4] and Hopp et al [5]. Contact angle measurements showed a correlation between radiation dose and surface free energy of all three polymers.

Acknowledgements

I would like to thank Dr. Brian Love for his advisement throughout the last five years. I would also like to thank the other two members of my committee, Dr. Nancy Love and Dr. Carlos Suchicital for giving of their time. I would also like to express my appreciation to the members of my research group, Sumitra Subrahmanyan, Scott Trenor, and Dr. Patricia Dolez for their help and advice with this and other projects. I would like to express my gratitude to Mark Makela of the Physics Department at Virginia Tech and Dr. Mool Gupta and Brandt Robertson of the Old Dominion University Applied Research Center for their help with performing laser ablation experiments. I would like to thank Robert Wimmer for developing and sharing with me his technique for cell culture and analysis on polymer surfaces. Finally, I would like to thank my sponsors throughout my time here at Virginia Tech: The National Science Foundation, The Center for Biomedical Engineering at Virginia Tech, The National Institutes for Standards and Technology, the U.S. Naval Costal Systems Command, and the Materials Science and Engineering Department.

Table of Contents

Page

1. Introduction ……1

1.1. Need for bioadhesion modulation……1

1.1.1. Implanted materials and biosensors…….2

1.1.2. Biofouling ……...2

1.2. Surface properties of biomaterials ……..3

1.2.1. Hydrophilicity ……4

1.2.2. Surface texture effects ……7

1.2.3. Inherent surface toxicity ……7

1.2.4. Culture environmental effects ……..…8

1.3. Modification of surface properties of polymers for biomedical uses ……..…9

1.4. Laser ablation for surface modification……..9

1.4.1. Morphological influences……..10

1.4.2. Surface chemical influences……..11

1.4.3. Roughening……....11

1.4.4. Poly(ethylene terephthalate)……..12

1.4.5. Poly(methyl methacrylate)…….……15

1.4.6. Polytetrafluoroethylene……..16

2. Experimental……..18

2.1. Materials selection…….18

2.2. Laser treatment…….……..21

2.3. Cell culture…….21

2.4. Contact angle…….25

2.5. Surface composition……...26

2.6. Surface topography……..…..26

2.6.1. Scanning electron microscopy……...……26

2.6.2. Optical microscopy……...…….27

2.7. Other materials characterization……...……..27

3. Results and Discussion……..27

3.1. Laser treatment……...…….28

3.2. Cell culture…….30
3.3. Surface energy……..…….33
3.4. Surface composition……..…….37
3.5. Surface topography……...……46
4. Conclusions..…….57
5. Future Work.……..58
6. References…….58
7. Appendix ……..63
8. Vita ……..67

List of Figures

Page

Figure 1 - Bubble configuration for measurement of contact angle at a liquid-solid-vapor interface 5
Figure 2 - Characteristic rolling structure generated on polymeric surfaces by laser ablation (polarized light micrograph of polypropylene foil irradiated at 193 nm and 0.1 J/cm^2) J. Breuer et al [49] 12
Figure 3 - Cone formation through laser ablation of polymer surfaces (SEM micrographs of PET after Kr-F laser ablation of 200-2000 pulses at 21 mJ/cm^2) Krajnovic [31]. 14
Figure 4 - Chemical structure of poly(methyl methacrylate)..... 15
Figure 5 - Chemical structure of polytetrafluoroethylene..... 16
Figure 6 - Laser ablation experimental setup (Virginia Tech)..... 20
Figure 7 - Cell culture experimental setup..... 23
Figure 8 - Contact angle measurement method 25
Figure 9 - Goniometer setup 26
Figure 10 – photograph of an ablated glycol-treated polyethylene terephthalate sample 28
Figure 11 – photograph of an ablated poly(methyl methacrylate) sample 29
Figure 12 – photograph of an ablated polytetrafluoroethylene sample 29
Figure 13 - Cell culture results ……..30
Figure 14 - Cell culture on an unmodified PMMA surface..... 31
Figure 15 - Cell culture results on Kr-F laser ablated PMMA surface (left). Surface structure shown on right..... 31
Figure 16 - Cell culture results on unmodified (left) and Kr-F laser surface treated PTFE 32
Figure 17 - Cell culture results on untreated (left) and treated (right) PETG..... 33
Figure 18 - Contact angle versus Kr-F laser treatment time for poly(methyl methacrylate) 34
Figure 19 - Contact angle versus dose for glycol-treated poly(ethylene terephthalate) ... 35
Figure 20 - Contact angle versus dose for polytetrafluoroethylene..... 36

Figure 21 - Results of surface free energy calculations from contact angle measurements as a function of dose for PMMA, PETG, and PTFE 37
Figure 22 - Chemical structure of poly(methyl methacrylate)..... 38
Figure 23 - XPS survey scan of treated and untreated poly(methyl methacrylate) 39
Figure 24 - Suggested mechanism of ablation for poly(methyl methacrylate)..... 39
Figure 25 - XPS multiplex scan of the C1s region of both treated and untreated 40
Figure 26 - XPS multiplex scan of the O1s region of both treated and..... 40
Figure 27 - Polytetrafluoroethylene chemical structure..... 41
Figure 28 - XPS survey scan of both treated and untreated polytetrafluoroethylene 41
Figure 29 - XPS multiplex scan of C1s peak of treated and untreated polytetraflurorethylene..... 42
Figure 30 - XPS multiplex scan of F1s region of both treated and untreated polytetrafluoroethylene 42
Figure 31 - Chemical structure of glycol-treated poly(ethylene terephthalate)..... 43
Figure 32 - XPS of C1s region of glycol-treated poly(ethylene terephthalate) 44
Figure 33 - XPS of O1s region of glycol-treated poly(ethylene terephthalate)..... 44
Figure 34 - XPS multiplex scan of glycol-treated polyethylene terephthalate 45
Figure 35 - Schematic of microscopy areas for Figures 36 through 38..... 46
Figure 36 – Micrograph of the center of the ablated poly(methyl methacrylate) surface (10x)..... 46
Figure 37 – Micrograph of the center of the ablated poly(methyl methacrylate) area (20x) 47
Figure 38 – Micrograph of poly(methyl methacrylate) sample at the boundary of the treated area 48
Figure 39 - SEM of poly(methyl methacrylate) surface ablated at 1000 mJ for 20 pulses 48
Figure 40 - SEM of poly(methyl methacrylate) surface ablated at 1000 mJ for 20 pulses 49
Figure 41 – SEM of poly(methyl methacrylate) surface ablated at 1000 mJ and 20 pulses 50
Figure 42 - SEM of polytetrafluoroethylene surface ablated at 1000 mJ for 1 pulse..... 50

Figure 43 - SEM of polytetrafluoroethylene surface ablated at 1000 mJ for 1 pulse 51
Figure 44 - SEM of polytetrafluoroethylene surface ablated at 1000 mJ for 20 pulses ... 52
Figure 45 - SEM of polytetrafluoroethylene surface ablated at 1000 mJ for 20 pulses ... 52
Figure 46 - Micrograph of the boundary of the polytetrafluoroethylene ablated area..... 53
Figure 47 - Feature size distribution for PMMA and PTFE treated at 1000 mJ for 20 pulses of Kr-F laser radiation..... 54
Figure 48 - SEM of glycol-treated poly(ethylene terephthalate) surface ablated at 1000 mJ for 20 pulses 55
Figure 49 - Micrograph of edge of glycol-treated poly(ethylene terephthalate) ablated surface 55
Figure 50 - Micrograph of crystallite on PETG ablated surface..... 56
Figure 51 - Micrograph of crystallites on ablated PETG surface 57
Figure 52- Sample DSC plot of heat flow versus temperature for glycol-treated poly(ethylene terephthalate)..... 64
Figure 53 - Stress versus strain for glycol-treated poly(ethylene terephthalate) in tension 65
Figure 54 - Stress versus strain for polytetrafluoroethylene in tension 66

List of Tables

Page

Table 1 - Materials specifications 18
Table 2 - Equipment specifications for lasers used in the treatment of the polymer specimens 19
Table 3 - Materials and suppliers for cell culture experimentation and analysis 21
Table 4 - Rich media formulation 22
Table 5 - M9 salt solution formulation 24
Table 6 - Cell stain solution formulation 25
Table 7- XPS peak assigments for curve-fitted C1s photopeak 38
Table 8 - Relative percent concentration of elements as determined by XPS 45
Table 9 - Experimental and published glass transition temperatures for PETG, PMMA, and PTFE 65
Table 10 - Modulus calculations from tensile strength testing of PMMA, PETG, and PTFE 67

1. Introduction

1.1. Need for bioadhesion modulation

1.1.1. Implanted materials and biosensors

1.1.2. Biofouling

1.2. Surface properties of biomaterials

1.2.1. Hydrophilicity

1.2.2. Surface texture effects

1.2.3. Inherent surface toxicity

1.2.4. Culture environmental effects

1.3. Modification of surface properties for biomedical uses

1.4. Laser ablation for surface modification

1.4.1. Morphological influences

1.4.2. Surface chemical influences

1.4.3. Roughening

1.4.4. Poly(ethylene terephthalate)

1.4.5. Poly(methyl methacrylate)

1.4.6. Polytetrafluoroethylene

1.1 Need for bioadhesion modulation

As technology advances, the need for materials with predictable cellular interaction intensifies. There is a shift in medicine toward materials that not only produce no negative foreign body response, but now actually promote cellular integration into the substrate [6]. Cellular monolayers are more progressively being implemented in biosensor applications, making the need for materials with positive cell-surface interactions increase. Other instances such as in food processing and marine applications demand a surface that will prevent cellular adhesion as a means of fouling resistance [7].

1.1.1. Implanted materials and biosensors

There are two potentially desirable *in vitro* responses for biomaterials in medicine. The first, more common, response is a passive one in which the implanted material is compatible to the point of not instigating an inflammatory response. Such a response could result in excess scar tissue formation, thrombosis, delayed proliferative response, and even early implant failure [8]. The second desired response for implanted biomaterials is the promotion of tissue integration. This type of response has been produced in all forms of materials from polymeric hydrogels [8] to nanoporous metals [9], to ceramic bone-integration materials.

In certain cases of implantation as well as in biosensor applications, some host response is desired. Cell seeding on implanted materials may actually help the implant material's introduction to the host environment. Dialysis tubing is one example of such a system [1]. By cell seeding the polymeric tubing, the administration of high volumes of heparin (anticoagulant) to the patient may be avoided. In the case of biosensors, bacterial properties may be harnessed as natural detectors for unnatural toxins or contaminants. In the study by Wimmer et al., *E. Coli's* natural response of potassium ion release was harnessed to develop a black-box device for toxin detection. The potassium ions were emitted from the bacterial cytoplasm through the activation of the glutathione-gated K+ efflux system. In this study, *E. Coli* was cultured on a glycol-treated poly(ethylene terephthalate) surface into which a micro fluidic channel was either laser-ablated or hot-imprinted. A K+-selective optical sensor was then attached to the microfluidic devise for detection of effluxed ions. Bacterial adhesion was promoted by laser ablation as well as oxygen plasma treatment [10].

1.1.2 Biofouling

With biofouling, whether by barnacle formation in nautical applications or bacterial growth in medical applications, the desire is to develop a surface capable of deterring any and all cellular adhesion or growth. To this end, numerous studies have been completed to establish what factors determine cellular or bacterial adhesion and

growth. Everything from surface energy and chemistry to surface texture has been examined to ascertain what exactly makes cells and bacteria adhere to surfaces [6, 7, 9, 11-26]. While the characteristics that modulate cellular adhesion depend on the individual cell properties as well as the temperature and flow patterns around the culture site, there exist some commonalities that can be used to predict cellular interactions. These shared characteristics are described below.

1.2. Surface properties of biomaterials

The surface properties of materials for biological applications can vary greatly depending on the application, the cells or bacteria involved, the toxicity of residual surface groups, surface texture, as well as the environment in which the material is required to perform. Much work has been done to predict and modify the adhesion of cells and bacteria to polymeric surfaces by cell or material selection, modification of the surface chemistry or texture, and modifications of the temperature and flow characteristics at the polymer surface. Biocompatibility is often critical for efficiency and even survival of an implant. If the material surface is cationically charged or toxic, the adjacent cells in contact with it can be physically or chemically damaged [1]. Depending on the cell and surface character, damage due to surface toxicity can range from cell rupture to cell death. Damage of the surrounding soft tissue can lead to necrosis causing pain, inflammation, and perhaps rejection or failure of the implant. In instances where the implanted material contacts hard tissue, the desired response is the promotion of cellular interaction as a means of bone ingrowth. Such is the case with bone-bonding polymers. These materials need relatively high strengths to be used as replacement tissues for ligaments and tendons and yet need to be capable of bonding for extended time periods to bone structures. Polymer hydrogels with an added bioactive hydroxyapatite component have been developed for these applications. The same bone-bonding characteristics have been achieved through surface modification of hydrophobic bulk polymers as well [1]. In the case of marine biofouling [7], [15], and even food processing [20], the purpose of surface treatment is to create a surface that will deter and perhaps even kill bacteria that come in contact with it. Grafting or copolymerization of

toxic functional groups to the surface material, development of adhesion-deterring surface morphologies, or targeted modifications of polymer hydrophobicity may accomplish this task.

1.2.1 Hydrophilicity

Much effort has been put into the effects of hydrophilicity on cellular or bacterial adhesion to surfaces. This research may be divided into two sub-groups: the characterization of cell or bacterial hydrophilicity and the characterization of substrate material hydrophilicity. Contact angle measurements are a common means of estimating thermodynamic parameters of surfaces. The two-liquid method allows for the approximation of the thermodynamic properties through the equations of Young, Dupre, and Zisman. The derivation of the Young-Dupre equations begins with a definition of the reversible surface free energy change per unit area of the new interface formed when a solid comes in contact with a liquid shown in Equation 1.

$$G_{SL} = \gamma_{SL} - \gamma_S - \gamma_{LV} = -W_A \qquad (1)$$

Where γ_S is the surface free energy of the solid in a vacuum, γ_{LV} is the surface tension of the liquid in equilibrium, γ_{SL} is the interfacial tension, and W_A is the thermodynamic work of adhesion. When combined with the equation of Young, which resolved vectorally the tensions at the interfaces (defined as γ_{LV}, γ_{SV} , and γ_{SL}) of a three-phase contact line (Eq. 2), the Young-Dupre equation is obtained (Eq. 3).

$$\gamma_{LV} \cos \theta = \gamma_{SV} - \gamma_{SL} \qquad (2)$$

$$W_A = \gamma_{LV} (1+ \cos \theta) + \pi_e \qquad (3)$$

The π_e term is defined as the equilibrium osmotic pressure, a term which is commonly assumed to be zero for polymers. The estimation for surface free energy developed through the work of Fowkes, Kaelble, Uy, Owens, and Wendt, which distinguished the

separate contributions of polar (depicted by ^{p}), dispersion (depicted by ^{d}), and hydrogen-bonding interactions of the two phases resulted in the geometric mean expression shown in Equation 4.

$$\gamma_{SL} = \gamma_S + \gamma_{LV} - 2(\gamma_S^d \gamma_{LV}^d)^{1/2} - 2(\gamma_S^p \gamma_{LV}^p)^{1/2} \qquad (4)$$

When combined with the Young-Dupre equation (3), and neglecting the π_e term, the following equation is obtained (5), which allows for the estimation of the surface free energy by solving a system of two equations for γ_S^p and γ_S^d.

$$\gamma_{LV}(1+\cos\theta) = 2(\gamma_S^d \gamma_{LV}^d)^{1/2} + 2(\gamma_S^p \gamma_{LV}^p)^{1/2} \qquad (5)$$

The surface free energy, γ_S is then calculated by simply adding γ_S^d and γ_S^p [27].

$$\gamma_s = \gamma_s^d + \gamma_s^p \qquad (6)$$

The two equations used to solve for the dispersion and polar portions of the surface free energy are obtained by taking contact angle measurements using two different liquids. Such measurements can be taken with a goniometer. This apparatus allows for the precise measurement of the angle at which a liquid bubble contacts a surface as shown in Figure 1 below.

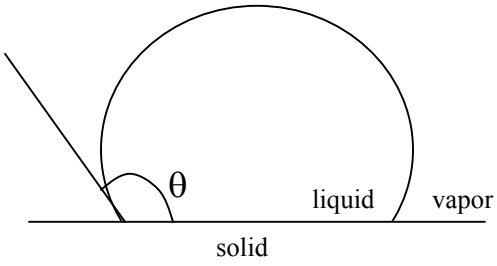

Figure 1 - Bubble configuration for measurement of contact angle at a liquid-solid-vapor interface

In the study by van Loosdrecht et al, contact angle measurements were taken on 23 different bacterial strains collected on microfilters. In the bacteria studied, contact angles with water ranged from 15° to 70° (*Escherichia Coli* K-12 water contact angle was 24.7° ± 0.4°) [25]. The characterization of cell wall hydrophobicity is important as it affects adhesion to surfaces and can therefore be a determining factor in materials selection for materials exposed to biological environments.

Cell wall hydrophobicity is only part of the interaction between cell and substrate. For this reason, numerous studies have been completed to characterize the hydrophobicity, as well as the effects of modifying the hydrophobic attributes of polymer surfaces for biological applications. Depending on what type of cell or bacteria is being attached to the substrate, different substrate hydrophilicities may be desired. For example, good adhesion of human endothelial cells [28], platelets [29], and Chinese hamster ovary (CHO) cells [18] were observed on hydrophilic polymeric surfaces (PET and PTFE). However, on a laser-induced acrylamide-grafted ethylene-propylene rubber and 2-hydroxyethyl methacrylate-grafted ethylene-propylene rubber, increased hydrophilicity decreased the long-term macrophage attachment when implanted in intramuscular and peritoneal tissues. The long-term attachment characteristics observed in this study were measured through 8-week *in vivo* experiments in the intramuscular and peritoneal layers of rabbits [21]. Other studies were inconclusive as to the effect of hydrophilicity on cell attachment because of other effects such as induced surface roughness, surface functional group modification, and changes in morphology. This was the case in the study by Cote et al on the *in vitro* analysis of cross-linked collagenous biomaterials [11]. No correlation between wettability and cell attachment was found by Jenney and Dadsetan of surface-coupled polyethylene oxide and laser surface modified poly(ethylene terephthalate), respectively [17,29]. Yet another study showed selective adhesion based on hydrophilicity when materials with similar surface textures were placed in culture together [13]. From previous research, it seems that cellular adhesion depends on the hydrophilicity of both the substrate and the cell wall, meaning that cell selection is just as important as material selection. When attempting to predict cell or bacterial attachment behavior, one must consider all aspects of the surfaces involved including hydrophilicity, roughness, toxicity and environmental effects.

1.2.2. Surface Texture Effects

Surface texture is known to affect cell and bacterial adhesion by mechanical means. Holes or grooves may actually serve as microreactors for cellular culture, meaning that they foster cellular adhesion and growth by allowing an extended cell-substrate interaction through reduction in the localized Reynolds number, particularly in high shear environments. For this reason, surface microfabrication has become an integral part of the design process for biosensors and micromachines [19]. The study by Matsuda and Chung used UV excimer lasers to ablate microholes in polyacrylamide that were subsequently put into culture with endothelial cells. These microholes 10 μm and 50 μm in diameter and 10 μm deep, successfully acted as microreactors for cell culture and are promising for use in medical diagnosis. One single endothelial cell was able to reside in a 10 μm diameter hole. Other studies have shown that cells will culture selectively on patterned or textured surfaces [6,12,13,29]. It is essential to recognize the importance of surface texture on cell adhesion, as texture effects are one consistent side-product of laser ablation of polymers.

1.2.3. Inherent surface toxicity

Particularly when working with surface treated polymers, surface toxicity effects are of concern. The remnants of laser ablation, plasma etching, surface grafting, or other means of surface modification may be toxic when cells are introduced adjacent to the residue. Certain levels of surface toxicity may however, be desirable. Prediction of the toxicity is important in materials selection and subsequent treatment. In the study by Wimmer et al, the treatment of polymer substrates with ammonia and oxygen plasma greatly modified the bacterial attachment of *E. Coli* K-12. While ammonia plasma treatment deterred the bacteria from attaching to the polymer surfaces, O_2 plasma treatment left enough oxygen on the substrate to promote bacterial attachment and growth [10]. Another study correlated the *in vitro* cytotoxicity of poly(propylene fumarate-co-

ethylene glycol) hydrogels to the molecular weight of the poly(ethylene glycol) used in the hydrogel development [8]. While toxicity is desirable for reducing biofouling in functions such as food manufacturing facilities and marine applications, too much toxicity in implanted materials can result in thrombosis and delayed proliferative response. Low levels of toxicity may be helpful in implanted materials by preventing a severe inflammatory response through disruption of the adhesion of monocytes and macrophages. Because the window of tolerable toxicity of implanted materials is so small, prediction of surface treatment effects and inherent toxic surface functional groups is extremely important.

1.2.4. Culture environmental effects

Another determining factor in biological adhesion to polymeric substrates is the culture environment. A study by Gallardo-Moreno et al measured the effect of temperature on the physiochemical surface properties and adhesion of *Enterococcus faecalis* [14]. Water, formamide, and diiodomethane contact angles were measured on bacterial lawns at different temperatures. This study showed that in the temperature range of 22°C to 37°C, cell hydrophobicity increased with increasing temperature. This increase in hydrophobicity correlated directly with the observed adhesion to glass and silicone substrates performed in this study [14]. Another process parameter known to alter cellular adhesion is the flow characteristics of the culture environment. There is an observed critical shear stress, which is substrate-dependent that must be achieved for good adhesion. In the study by Horbett et al of cellular adhesion to different hydroxyehylmethacrylate copolymers, critical shear stresses ranged from 0-18 dynes/cm^2, depending on the strength of the cell-substrate interaction [16]. When values of surface shear stresses were at or near this observed critical value, the highest rate of adhesion was observed.

1.3. Modification of surface properties of polymers for biomedical uses

Because most materials do not exhibit both the surface and bulk demands required for use in biomedical applications, surface modification has been identified as an effective approach to producing the desired cellular response without compromising the bulk material characteristics [1]. Three surface parameters that may be modified to produce the desired response are the morphology, the surface chemistry, and the surface roughness. The morphology of poly(ethylene terephthalate), can be changed from crystalline to amorphous through laser ablation [30]. Desirable surface groups may be added to a material through numerous surface treatments including oxidation, ion implantation, graft polymerization, laser ablation, and plasma modification [1]. This study focused on laser ablation as a means of surface modification for biological purposes.

1.4. Laser ablation for surface modification

Laser ablation as a means of polymer surface treatment offers modification of the morphology, chemistry, and texture of the surface material. The type and extent of modification depends upon several factors including the laser wavelength and fluence, the absorption index of the polymer at the laser wavelength, and the atmosphere in which the treatment occurs. The influence laser exposure has on a polymeric surface depends on the mechanism of ablation of that particular material. If the polymer is strongly or weakly absorbing at the laser wavelength, two independent classes of ablation behavior have been identified [31]. For strongly absorbing polymers, a phenomenological etch rate can be determined which is directly related to the laser fluence and pulse duration [32]. However, in weakly absorbing polymers, there is a different phenomenon associated with ablation. Prior to ablation, there is an incubation period in which the polymer absorbs energy that is followed by side-chain scission resulting in a less-saturated backbone and stronger UV absorber [31]. A study by Efthimiopoulos, *et al.*

showed that with weakly absorbing polymers, the incubation period can lead to superheating of the surface material followed by volumetric bubble creation [2].

The laser used in this study was a KrF excimer laser at 248 nm. At this wavelength, PMMA was a known weak absorber, while PET is a strong absorber and the absorption characteristics of PTFE were unknown. The absorption index of the polymer at the laser wavelength defines the mechanism of photoablation [33]. Several studies however, have revealed that the characteristic rolling structure associated with ablation can be achieved in low absorption index polymers by simply applying a higher radiation dose [31,34,35].

The laser beam fluence is also key in predicting ablation behavior in polymeric structures. While fluences below the critical threshold fluence may be effective in modifying surface chemistry and even morphology, for material removal and true ablation to occur, the threshold fluence must be reached. For weakly absorbing polymers, it may take several laser pulses to reach the ablation threshold, while in strongly absorbing polymers, material removal can take place with the first pulse.

1.4.1 Morphological influences

Morphological changes, or modifications of the crystal structure of a material, are one natural side effect of laser ablation. In more highly crystalline polymers such as poly(ethylene terephthalate), surface amorphization has been observed [30]. In other instances, such as the development of poly(tetrafluoroethylene) films through laser ablation and deposition, the laser initiated crystallization in a primarily non-crystalline polymer [36]. When polymers are irradiated, much of the energy is converted into heat. Depending on the intensity of the radiation, the surface material may be heated to above its softening temperature. Depending on the duration of treatment, the molten surface material may then either be essentially quenched into its amorphous state, or allowed to cool more slowly, resulting in a more ordered semi-crystalline state. The resulting surface morphology may be controlled or predicted through proper material and treatment selection.

1.4.2. Surface chemical influences

Surface chemistry effects associated with laser treatment are still somewhat unresolved. While there have been definable changes in all polymers, the ability to characterize the chemistry occurring is speculatory, depending on individual interpretation of the data. While some studies indicate that most ablation products consist primarily of monomer fragments (PET and polyimide) [32], other studies have observed breakdown of the polymer into reactive surface groups, incorporation of the ablation atmosphere into the surface material, and even defluorinization in the case of PTFE [36-38]. The mechanism of surface chemistry modification is still somewhat undecided due to conflicting results of different studies.

1.4.3. Roughening

Surface texture effects of laser irradiation are certainly a concern in any materials application, but particularly in biological applications where mechanical adhesion can be the primary means of cellular attachment. Laser ablation has been shown to produce a characteristic rolling texture effect in a number of polymers including PET [4,5], poly(ether ether ketone) [39], polyimide, [33], poly(acrylamide) [19], polyethylene [40-41], bisphenol-A polycarbonate/PMMA blends, polycarbonate/PMMA blends [42] and poly(butyl terephthalate) [43]. All of these polymers displayed the same repeated rolling surface structure following ablation. Theories behind the source of this rolling structure are varied. One study assumes that the rolling structure is due to thermal shock waves that are traveling through the surface material due to the immense energy introduced [4]. An example of this type of rolling structure is shown in Figure 2 below. In fluid flow situations, the valleys in between protruding surface materials would be adequate for enhancement for biological attachment through mechanical means.

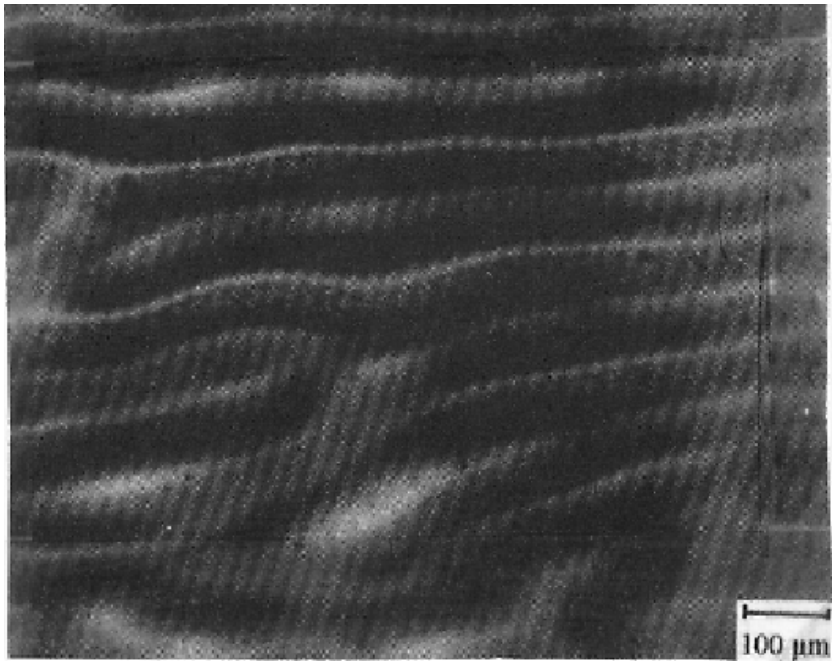

Figure 2 - Characteristic rolling structure generated on polymeric surfaces by laser ablation (polarized light micrograph of polypropylene foil irradiated at 193 nm and 0.1 J/cm^2) J. Breuer et al [49]

Poly(methyl methacrylate) demonstrates an entirely different surface topography following ablation. PMMA ablates through subsurface superheating, meaning that the material heats above its softening point below the surface, degrades and releases dissolved gases that create subsurface explosions. This mechanism of ablation results in the overall destruction of the surface material into a cratered structure with significant debris formation. The modification of the surface in this way should promote biological attachment by the same mechanical means described in Section 1.4.3 previously.

1.4.4. Poly(ethylene terephthalate)

While there is little to no published research on laser ablation of the glycol-modified poly(ethylene terephthalate) used in this study, much research has been conducted on ultraviolet laser ablation of PET, or Mylar^{TM}. PET is classified as a strongly absorbing organic polymer in the UV range, grouping it with other polymers

such as Kapton™ [32]. Strongly absorbing polymers exhibit zeroith-order ablation characteristics, meaning that once the critical ablation threshold is reached, the rate of ablation is independent of pulse number. There is also a logarithmic relationship between the ablation rate and fluence above the critical fluence [31]. Several surface effects with the potential to modulate cellular adhesion have been identified and linked to laser treatment of poly(ethylene terephthalate) including amorphazation of the surface material, surface chemical changes including, but not limited to increased hydrophilicity, and surface texturing [3-5, 30, 32, 44].

Lasare and Benet [30] phenomenologically describe the amorphization of PET due to laser treatment. This study used ellipsometry to describe a characteristic amorphization of the surface material of a 60% crystalline PET film by irradiation with both ArF and KrF excimer lasers. This behavior is consistent with ablation theories of strongly absorbing polymers mentioned previously. The front edge of a pulse of radiation is absorbed by a volume of surface material determined by the pulse fluence and the absorption characteristics of the material. This volume of surface material will eventually vaporize. The resulting plume of vaporizing gas partially blocks the remainder of the pulse, only allowing some of the remaining energy to pass through to the newly created polymer surface. The energy transmitted to the new surface is then primarily converted into heat, often reaching temperatures above the melting point of the polymer (around 265°C for PET [45]). Due to the short span of the radiation treatment, the surface then undergoes a quench, freezing an amorphous structure into an otherwise relatively crystalline polymer.

In another study by the same group, surface chemistry effects were also observed with ablation. There was an observable drop in the oxygen to carbon ratio with ablation as measured by x-ray photoelectron spectroscopy [30]. The drop in the O/C ratio is consistent with the breaking of the polymer chain at the ester functional group site. In the Lazare study, the photolysis resulted in an oligomeric surface layer that was soluble in acetone, whereas the untreated polymer was not. Another study by Dadsetan et al, confirmed the amorphization of the surface structure, but suggests that the bond breaking with Kr-F laser ablation happens at the bond between the carbonyl and the aromatic ring in the PET chain (determined by attenuated total reflectance infrared spectroscopy).

Contact angle measurements were performed in this study that showed a correlation between hydrophilicity and radiation dose in PET [29]. The increase in hydrophilicity of the ablated surface is due to the formation of radicals capable of converting into hydrophilic groups when in contact with air.

Despite conflicting opinions on what chemical effects occur on the PET surface during excimer laser ablation, there is agreement on the development of texture during ablation. With ablation, a regular, textured surface is formed with feature sizes on the order of microns. The developed surface structures are described as "rolls" or "cones," and are laser fluence dependent as well as dose dependent, with the structures becoming more prominent with additional radiation. These surface structures were observed with scanning electron microscopy, optical profilometry, atomic force microscopy, and scanning tunneling microscopy [4, 5, 29, 32]. An example of the formation of conical structures on polymer surfaces with laser ablation is shown in Figure 3, below.

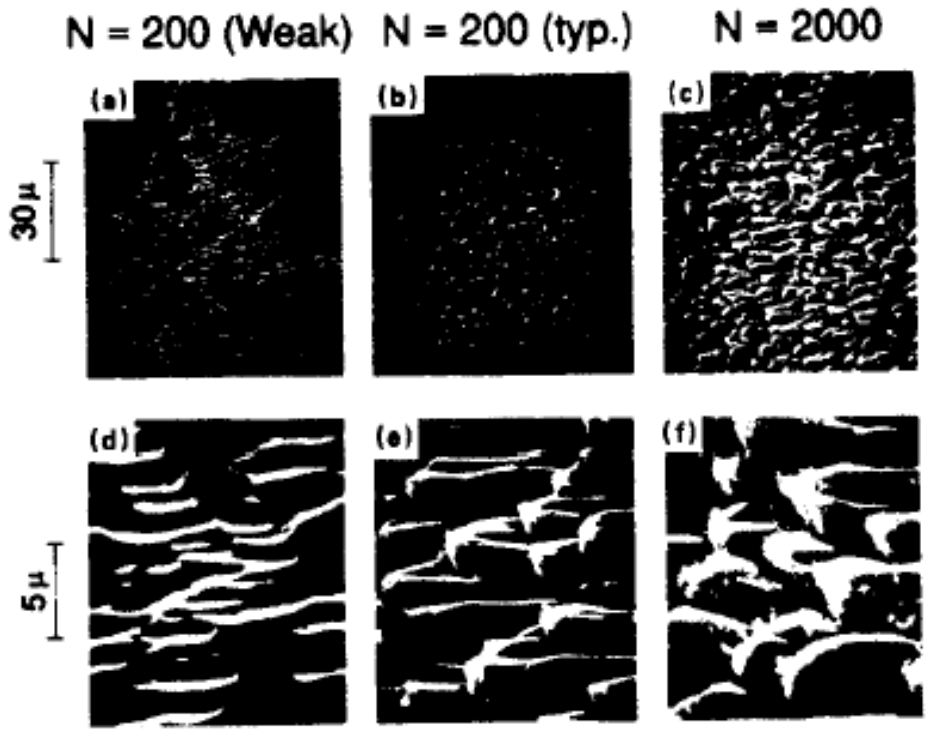

Figure 3 - Cone formation through laser ablation of polymer surfaces (SEM micrographs of PET after Kr-F laser ablation of 200-2000 pulses at 21 mJ/cm^2) Krajnovic [31]. N corresponds to the number of laser pulses delivered.

The conical structures form because of the temperature gradients in the superheated surface material. The temperature gradients in combination with the brevity of the radiation dose result in molten portions of surface material that flow by convection around more dense portions of material. The result is a structure that has a regular surface structure [5]. This type of microfabricated surface structure has been shown to provide adequate reactor sites to promote adhesion of endothelial cells [18].

1.4.5. Poly(methyl methacrylate)

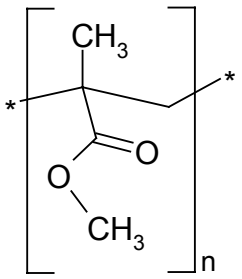

Figure 4 - Chemical structure of poly(methyl methacrylate)

The mechanism for ablation in the case of poly(methyl methacrylate) is very different from that of PETG. While the laser radiation is converted into heat in the same manner, there is evidence as presented by Efthimiopoulos et al. to suggest that the superheating of the surface material causes acoustic waves due to the material's inherent elasticity. These acoustic waves lead to the development, aggregation, and subsequent bursting of microscopic bubbles resulting in the violent removal of surface material. This removal is dose dependent as well as dose intensity dependent. At low energies, a sequence of pulses may form, aggregate, grow, and finally explode these bubbles. When the energy is increased, a single pulse may form, aggregate and grow the bubbles, with only one additional dose required for the bubbles to burst. Finally, at high energies, all of the steps needed for significant material removal through volume bubble formation take place with a single pulse [2].

While the study by Efthimiopoulos et al describes ablation of PMMA above the ablation threshold, there are alternate theories regarding the ablation behavior of PMMA at lower energies. One of these theories suggests that because PMMA is weakly absorbing at 248 nm ablation occurs first through an incubation followed by subsequent ablation. During the incubation period, the material is converted either photochemically or thermally into a more highly absorbing material. The modified material then ablates as if it were strongly absorbing at that wavelength [31]. The degradation of PMMA through photochemical reactions into methanol, carbon monoxide, and methyl formate was confirmed in the Krajnovich study through photofragment translational spectroscopy. This study suggests that the bubble formation seen at higher radiation doses could be due to the evolution of the gases formed during incubation. And yet, while the mechanism of ablation remains up for debate, one thing remains unquestioned; laser surface treatment has a significant effect on the wettability characteristics of poly(methyl methacrylate).

One study of the surface characteristics of PMMA by various laser irradiation revealed that KrF excimer laser radiation improved the wettability as measured by contact angle. This change in contact angle is contributed to the increase in surface oxygen with ablation (surface analysis completed by XPS). The study by Lawrence et al asserts that the increase in surface oxygen content observed by XPS is due to the formation of some level of O_2 –containing polar functional groups [46]. The presence of these groups in combination with the drastic change in surface texture explains the modulation in surface energy of the ablated material.

1.4.6. Polytetrafluoroethylene

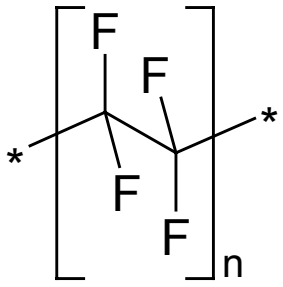

Figure 5 - Chemical structure of polytetrafluoroethylene

The chemical surface modification of polytetrafluoroethylene has become of much interest in recent years for possible electronic materials applications as well as biological applications. PTFE provides a low dielectric, chemically resistant and heat stable material. The only difficulty encountered with its use in electrical applications is its resistance to metallization [38]. In an attempt to rectify this problem, much effort has been put into surface modification of PTFE by various means, including laser ablation. In the study by Norton et al, laser ablation was used as a means of thin film deposition. A very high fluence of 9 J/cm^2 was used to deposit ablated material to various substrates including glass microscope slides, single crystal silicon wafers, carbon-coated copper grids, single crystal NaCl, and single crystal KBr. This study found that at above 200°C, ordered semi-crystalline films were formed, while at temperatures below 200°C, amorphous PTFE films were formed [36]. While contact angle measurements of the films were not conducted in this particular study, the morphology of the films must certainly affect their inherent hydrophilicity.

Other studies of the surface treatment of PTFE by excimer laser ablation showed changes in contact angle that correlate to both the fluence and dose of radiation. When PTFE is irradiated in the presence of oxygen, as in the study by Girardeaux et al, not only is there an observed defluorinization, but some oxidized carbon species were also detected on the ablated surface [37]. The presence of surface oxygen and hydrocarbon contamination in combination with the decreased fluorine content is an important modification of the surface relevant to cellular adhesion. In the study by Niino, which focused on modification of PTFE for subsequent metallization, contact angle measurements revealed an increasingly hydrophilic surface with radiation dose as determined by water droplet contact angle. With 3000 pulses at 27 mJ/cm^2, the contact angle was lowered from an unmodified value of 130° down to 25°, a significant change in the naturally hydrophobic nature of this polymer. In this case, the surfaces were treated in the presence of hydrazine, which resulted in residual amino groups on the treated surfaces [38]. The ability to control the hydrophilic nature of polymers like PTFE through laser ablation is significant if these materials are to be developed further for a

broader variety of applications including biosensors, anti-fouling materials, biomedical implants, and electronics.

2. Experimental

2.1 Materials selection

2.2. Laser treatment

2.3. Cell Culture

2.4. Contact angle

2.5. Surface Composition

2.6. Surface Topography

2.6.1. SEM

2.6.2. Quantitative analysis of morphological features

2.7. Other general materials analysis for background purposes

2.7.1. Mechanical testing

2.7.2. DSC

2.1. Materials selection

Table 1 - Materials specifications

Material	**Supplier**
Polymethyl methacrylate 12” x 24” sheets, 1/8” and 1/16” thickness	McMaster-Carr
Polytetrafluoroethylene 12” x 24” sheets, 1/8” and 1/16” thickness	McMaster-Carr
Glycol treated polyethylene terephthalate 12” x 24” sheets, 1/8” and 1/16” thickness	McMaster-Carr

Three substrate materials: poly(methyl methacrylate) (PMMA), glycol-treated poly(ethylene terephthalate) (PETG), and polytetrafluoroethylene (PTFE) were selected for full evaluation. Two other materials, low-density polyethylene and poly(ether ether ketone) were selected for evaluation as well, but later eliminated from testing due to their

inherent fluorescence in the green and red wavelength regions discovered under fluorescence microscopy conditions. LDPE and PEEK were eliminated because this fluorescence made examination of the cell culture products impossible with the procedure used. PMMA and PETG were selected due to the differences in ablation characteristics as described by the literature. PTFE was chosen because of its wide use in biomedical applications and its little-known ablation characteristics. All of the materials were obtained in extruded sheet form in either 1/8" or 1/16" thicknesses from McMaser-Carr. Both the PETG and the PMMA sheets came with a protective cover sheet that was removed prior to treatment or examination by other means. Prior to ablation or other treatment, the materials were cleaned with deionized water and a Kimwipe. No solvents were used to clean the material surfaces so as to prevent any contamination of the surfaces with foreign organic functional groups. While it is possible that there were other metallic contaminants on the sample surfaces, these would be easily identified during the surface compositional analysis with XPS and steps to remove contamination without damaging the samples could be taken. This was not necessary however, as metallic contaminants did not prove to be an obstacle in these experiments.

2.2. Laser treatment

Table 2 - Equipment specifications for lasers used in the treatment of the polymer specimens

Equipment (Virginia Tech)	**Supplier**
Kr-F excimer laser model LPX300	Lambda Physik
Lens stepper motor model STP-57D317	Stepper Motor Controller
PLCX-50.8-154.5-UV-248 lenses	CVI Laser Corporation
Equipment (Jefferson Labs)	**Supplier**
Laser Excel 3000 Kr-F laser	Laser Excel

A Lambda Physik LPX300 Kr-F laser was used to surface treat each polymers. Initial exploratory experiments were run to determine optimal spot size and energy for ablation. Spot size was manipulated by varying the dimensions of an internal aperature. Three spot sizes as defined by the aperture (8mm x 3mm, 5mm x 2mm, and 3mm x 1.5 mm) and 5 energies (306, 438, 672, 900, and 1026 mJ) were used. Upon observation of the results of these experiments, the medium spot size 5mm x 2mm and maximum energy of approximately 1000 mJ were chosen for further experimentation. This choice of energy and spot size delivered a dose per pulse of 3.3 x 10^9 W/cm^2. This spot size and energy were chosen in order to maximize the area to be ablated while still producing results observable with the naked eye. With this energy and spot size there was a visibly observable modification of the surface of all three polymers.

Translation of the laser beam was done using a Stepper Motor Controller STP-57D317 mounted on a rastering lens. This stepper motor moved the lens 1.8° /step at a speed of 20 steps/min. The experimental setup is shown in Figure 6 below.

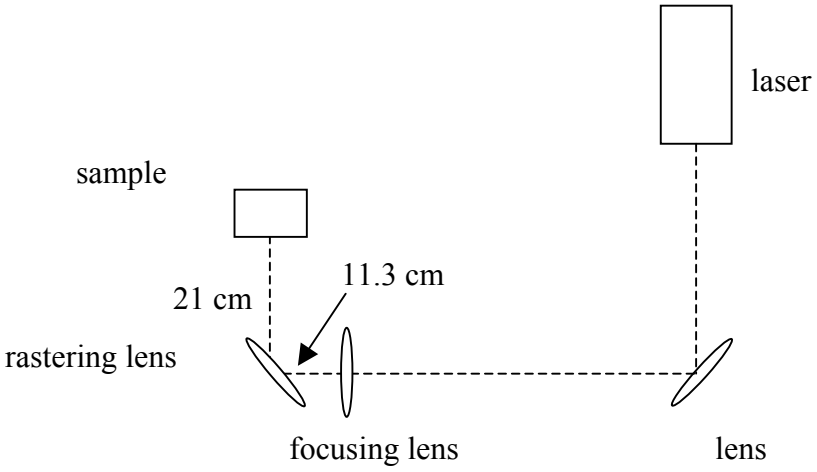

Figure 6 - Laser ablation experimental setup (Virginia Tech)

The distance between the rastering lens and the sample was 21 cm and the distance between the rastering lens and focusing lens was 11.3 cm. The laser was pulsed at 5 Hz as the beam translated across the polymer surface. All experiments were run in air with a fan to prevent ablation products from depositing on the rastering lens by blowing the

plume away. The plume formed was consistent with effects seen in previous experiments described in the introduction. Plumes associated with polymer ablation are typically caused by the vaporization of surface materials due to the fast heating of the surface material with radiation [30].

2.3. Cell culture

Table 3 – Materials, suppliers, and equipment used for cell culture experimentation and analysis

Material	**Supplier**
Sodium Chloride	Fisher Scientific
Tryptone or tryptone peptone	Fisher Scientific
Bacto™ Yeast Extract	Fisher Scientific
Na_2PO_4	Fisher Scientific
KH_2PO_4	Fisher Scientific
NH_4Cl	Fisher Scientific
LIVE/DEAD BacLight bacterials viability system	Molecular probes, Inc. Eugene, OR
Slide slip covers	
Fingernail polish	Tech bookstore
Eschericia coli K-12 ATCC #2382	ATCC, Manassas, VA
Microscope camera	Hamamatsu Orca
imaging software	Image-Pro Plus
Image Analysis software	Scion Image
IX50 Fluorescence Microscope	Olympus

The cell culture experimental setup was a modified Fisher cell developed by Wimmer et al. *E. Coli* K-12 bacteria were cultured in a rich media solution of the formula shown in Table 4. The sodium chloride, tryptone or tryptone peptone, and Bacto™ Yeast Extract were added to 3 liters of deionized water in a large beaker. A

magnetic stirbar was added to the solution that was then placed on a magnetic stirplate. A sponge stopper was put in the beaker and the solution was mixed until the powder components dissolved. The beaker and solution were then sterilized in an autoclave at 121°C for 1 hour.

Table 4 - Rich media formulation

sodium chloride	10 g/L
tryptone or tryptone peptone	10 g/L
Bacto™ Yeast Extract	5 g/L
deionized water	

Once the rich media solution was out of the autoclave, the culture was started in the rich media from a slant culture. The slant culture was made by streaking the *E. Coli* on solid LB media with 1.5% agar. A metal loop was sterilized by passing it over the Bunsen burner flame. The cap was then removed from the slant culture and the end of the test tube was passed over the burner flame. The metal loop was scraped across the surface of the slant culture and then drawn through the rich media. The end of the slant culture was then again passed across the burner flame and the cap replaced. The loop was then sterilized again by passing it across the burner flame. The rich media solution was then incubated in the water stir bath for 14 – 16 hours at ambient temperature, 23°C. Based on the growth curve for *E. Coli* K-12 from Wimmer et al [10], this incubation time put the bacteria in the log stage of growth. The log stage of growth was determined to be the best for promoting adhesion to polymeric substrates such as these in previous experiments conducted in collaboration with the Civil and Environmental Engineering Department of Virginia Tech.

To ensure that the culture was in the log stage of growth, culture absorbance was tested using a Bauch & Laumb Spec 20 spectrophotometer. Three milliliters of the culture was added to 3 mL of sterile media in a spectrophotometer tube. The culture mixture was then compared to uncultured sterile media in the Spec 20, yielding a

fractional absorption value. This value was then compared to an E. Coli K-12 growth curve to ensure that the bacteria were in the log stage of their growth.

Three 295 mL amber bottles were used to culture the cells on the polymer surfaces. Four 1" x 3" polymer samples were placed in each bottle and separated by a piece of plastic tubing. Holes were cut in the rubber stoppers and glass tubing inserted and secured with adhesive caulk. Plastic tubing was connected to the glass tubing and also sealed with adhesive caulk (see Figure 7). The tubing was run through a peristaltic pump with adjustable flow and the ends inserted into the rich media culture. Once the bottles fill up with solution, the peristaltic pump provided the flow velocity through the system necessary to ensure laminar flow (Re=10) within the bottles. The polymeric samples remained in culture for 3.5 hours.

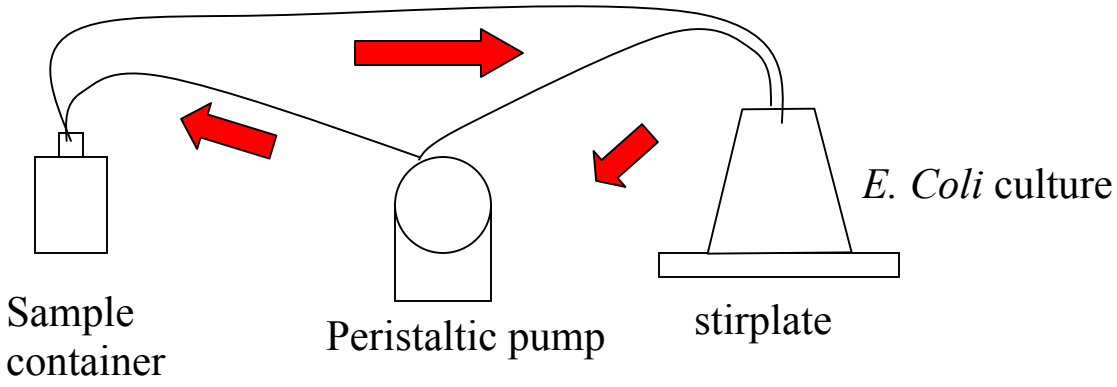

Figure 7 - Cell culture experimental setup

Once the cell culture was completed, the system was flushed using an M9 salt solution (formula shown in Table 5). This solution was passed through the sample bottles for one hour or until all of the solution was used. Rather than recycling the solution as with the rich media culture, the salt solution is pumped out for disposal. While the salt solution is running, a graduated cylinder is used to collect the fluid being pumped from the bottles. The flow rate is determined by measuring the volume of fluid pumped from each of the three bottles in one minute. As long as the flow rate remained between about 15-18 mL / min., laminar flow was assured. The bottles are then capped and the samples are ready for observation under the fluorescence microscope.

Table 5 - M9 salt solution formulation

Na_2PO_4	30g anhydrous, or 56g hydrous
KH_2PO_4	15g
NH_4Cl	5g
NaCl	2.5g
To these ingredients, add deionized water to 900mL, put on a stir plate overnight, then add deionized water to 1000mL to get M9 salt solution	
M9 salt solution	500mL
Sterile water	4.5L

The LIVE/DEAD cell stain was used to characterize the bacterial adhesion under the florescence microscope. The stain was prepared with the formulation shown in Table 6. Once mixed, the solution was kept in a foam tray to minimize light exposure. To prepare a sample for observation, the sample was slowly removed from the bottle containing the M9 flush solution. Using a micropipette, 15 μL of the stain solution was dropped onto the sample surface. A microscope cover slip was then dropped on the area where the dye solution was deposited. The cover slip was then adhered to the surface of the sample using fingernail polish. The sample was then placed in a dark area (desk drawer) where it was allowed to incubate for 15 minutes. The incubation time allows for the stain to permeate through the bacteria on the sample surface, allowing for detection by fluorescence microscopy.

Table 6 - Cell stain solution formulation

Deionized water	994 μL
Red dye	3 μL
Green dye	3 μL

Samples were observed using the Olympus IX50 fluorescence microscope with a 60x lens, a Hamamatsu Orca camera, and Image-Pro Plus imaging software. Using the appropriate fluorescence filters, a capture of both the live and dead cells was made and subsequently analyzed with Scion Image software.

2.4. Contact angle

Contact angle measurements were made using the two-liquid method with a goniometer. A DAGE video setup projected the stage onto a Javelin monitor. The stage was illuminated using a Fiber-lite source. A 25 μL microsyringe (Fisher) was used to dispense 5 μL of either deionized water or methylene iodide (CH_2I_2) onto the substrate surface. The contact angle was then measured as the angle between the substrate surface and the tangent to the drop at the point of contact as shown in Figure 8 below.

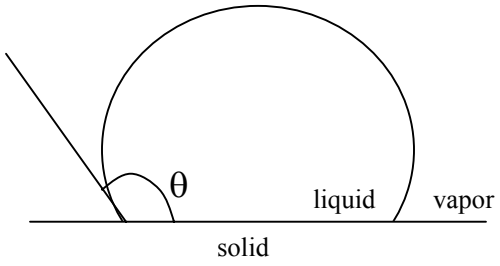

Figure 8 - Contact angle measurement method

A schematic of the goniometer setup is shown in Figure 9 below:

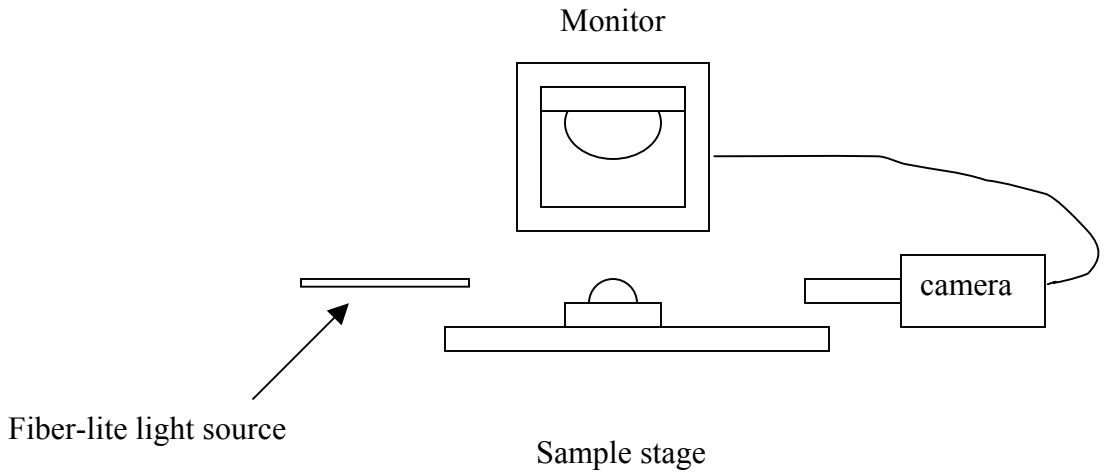

Figure 9 - Goniometer setup

2.5. Surface composition

Surface composition was determined through X-ray photoelectron spectroscopy (XPS) using a Cu Kα source and a pass energy of 44.75 eV. Both treated and untreated samples were cut down to approximately 1 cm x 1 cm squares and placed in the XPS. A glancing angle of 15° was used for treated samples and a steeper, 45° angle was used for untreated samples to determine surface composition. Both survey and multiplex scans were run and peak intensity versus binding energy was recorded.

2.6. Surface topography

2.6.1. Scanning electron microscopy

An ISI–SX-40 scanning electron microscope was used to characterize surface texture. Samples were coated with gold using a S150B Edwards Sputter Coater prior to their installation in the SEM. They were then individually placed in the vacuum chamber and the surface topography observed.

2.6.2. Optical microscopy

Optical microscopy was performed using an Olympus microscope with polarizing filters and digital camera attachment. Filters were configured to provide the greatest phase contrast for each sample observed.

2.7. Other materials characterization

2.7.1 Mechanical testing

Dogbone specimens were cut from each of the three materials as described in the ASTM standards. These samples were pulled in tension in a Texture Analyzer test frame at a rate of 1 millimeter per minute. Stress versus strain diagrams were generated from the force-deflection data collected with the Texture Analyzer system.

2.7.2. Differential scanning calorimetry

Small samples (8-20 mg) were cut from each of the three materials and placed in aluminum sample pans that were subsequently sealed. Samples were scanned through a range of temperatures with a Pyris Series 7 Differential Scanning Calorimeter. From the data obtained, the glass transition temperature was determined.

3. Results and Discussion

3.1. Laser treatment

3.2. Cell culture

3.3. Surface energy

3.4. Surface composition

3.5. Surface topography

3.1. Laser treatment

Samples for the majority of the study were treated using the Kr-F laser from Lambda Physik at 1000 mJ. This high intensity produced an ablation effect in all cases, with some charring occurring in the case of PTFE and PETG. Examples of ablation products are shown in Figures 10-12 below.

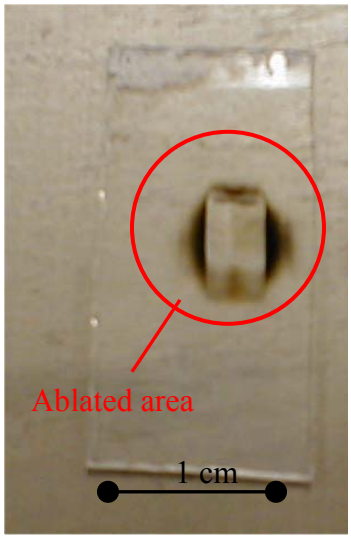

Figure 10 – photograph of an ablated glycol-treated polyethylene terephthalate sample

In the case of PETG, there was a significant visible gaseous plume coming off of the surface during treatment. There was also a loud "pop" associated with each laser pulse. The high moisture content of this particular material was thought to be the reason behind the sound associated with ablation. The ablated surface remained glassy clear, indicating no visible surface roughening with treatment.

PMMA, while not charred during ablation, displayed the highest ablation rate, with significantly more material coming off of the sample under the same ablation conditions. There was also visible surface roughening as well as a strong odor with radiation. As seen in Figure 11 the sample is less transparent in the ablated area.

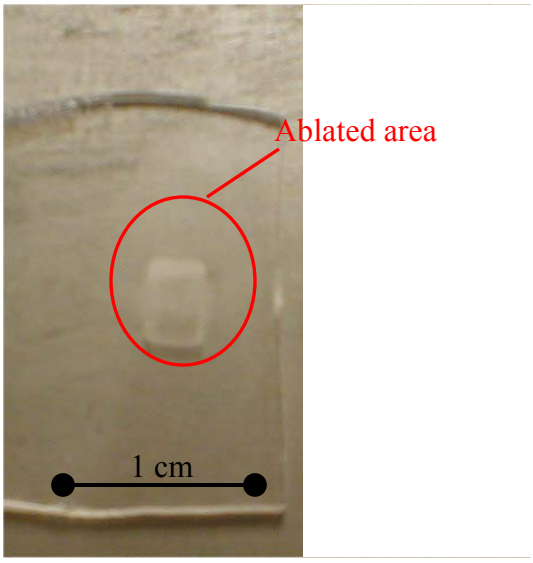

Figure 11 – photograph of an ablated poly(methyl methacrylate) sample

PTFE displayed the same charring effect around the edges of the treated sample as PETG. There were also some visible signs of surface roughening with ablation. While the initial surface impact was loud, subsequent pulses failed to produce the same level of noise. No plume was visible in this case. Figure 12 shows the results of laser ablation on a PTFE sample.

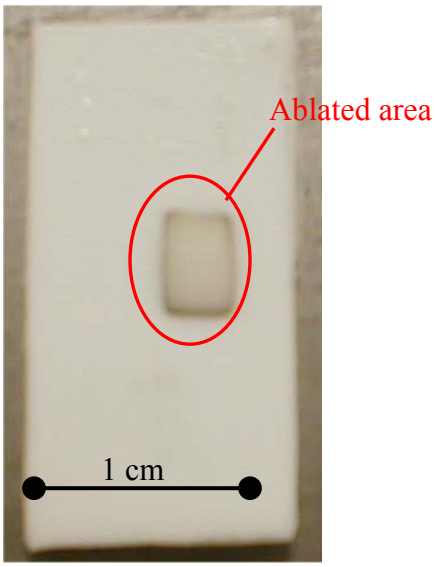

Figure 12 – photograph of an ablated polytetrafluoroethylene sample

3.2. Cell culture

As shown in Figure 13 there was a statistically significant difference in bacterial adhesion to all three polymer substrates following laser surface modification. While attachment was deterred in the PTFE and PMMA, it was somewhat enhanced in the PETG samples.

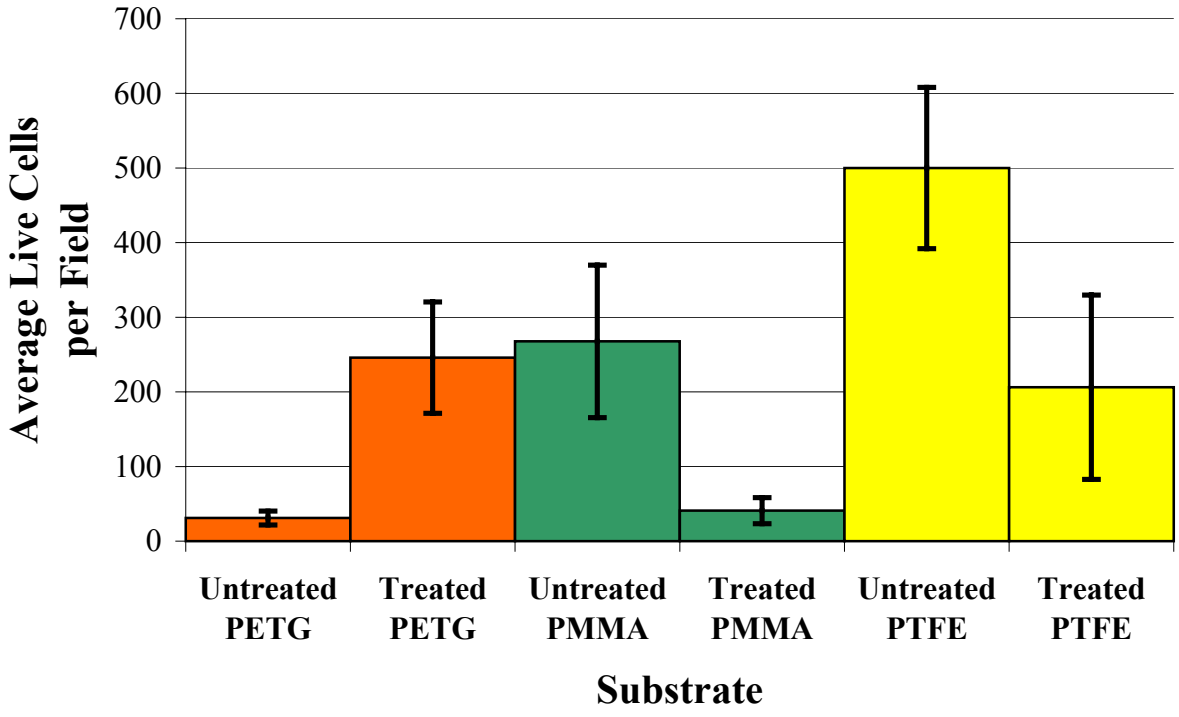

Figure 13 - Cell culture results

In the case of PMMA, which developed a crater-like structure with ablation, there was preferential cell attachment observed within the crater structures. Whereas there is a fairly uniform bacterial attachment on untreated PMMA, once the surface has been irradiated, the attachment is decreased and patchy. Figure 14 below shows attachment to an unmodified PMMA surface. Figure 15 shows culture results on a laser-ablated surface, with a micrograph in ambient light to its right to illustrate the preferential adhesion within crater structures.

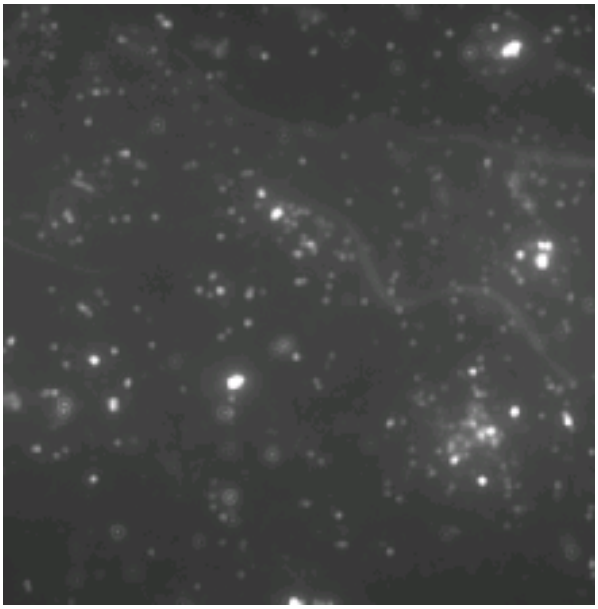

Figure 14 - Cell culture on an unmodified PMMA surface

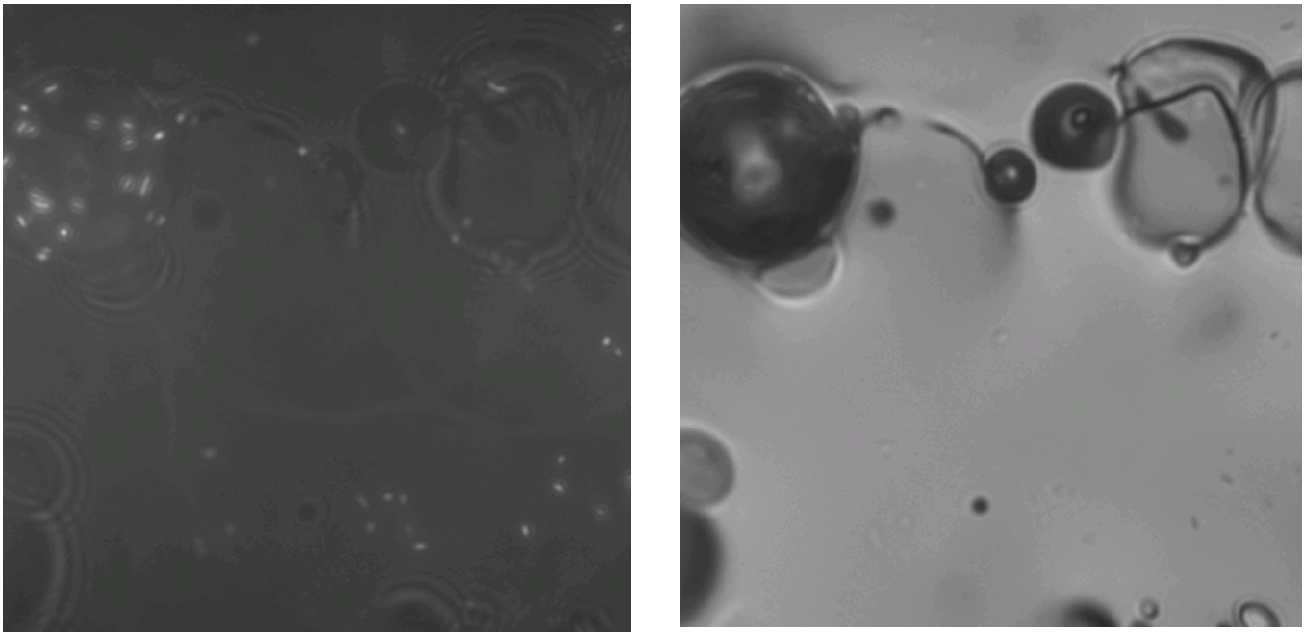

Figure 15 - Cell culture results on Kr-F laser ablated PMMA surface (left). Surface structure shown on right.

In the case of PTFE, the most noticeable difference in the cell culture results before and after laser irradiation was whether or not the bacteria clustered on the surface. Figure 16 shows the cell culture results of unmodified (left) and surface treated (right) PTFE. Notice the large bacterial clusters on the unmodified surface whereas the bacterial distribution is more uniform on the laser ablated surface.

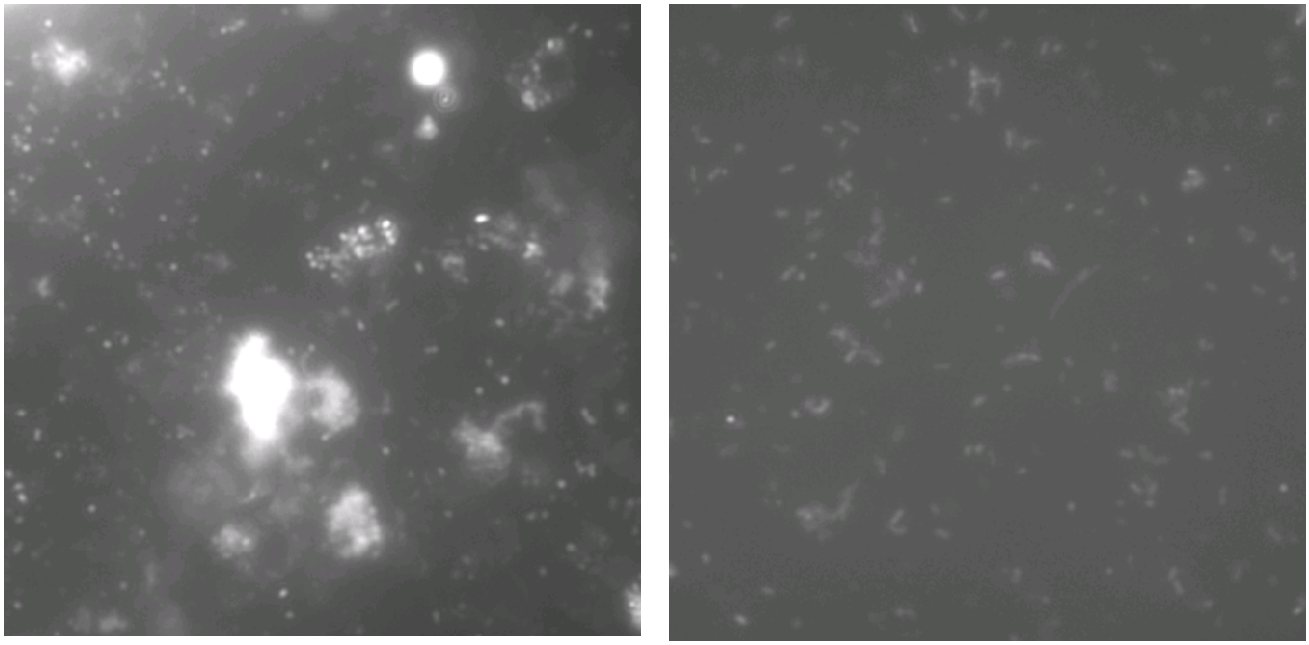

Figure 16 - Cell culture results on unmodified (left) and Kr-F laser surface treated PTFE (right).

Finally, in the case of PETG, there was no change in the distribution of the bacteria on the surface before and after treatment, however, the number of attached bacteria increased significantly after ablation. Figure 17 shows cell culture results for both untreated (left) and treated (right) PETG.

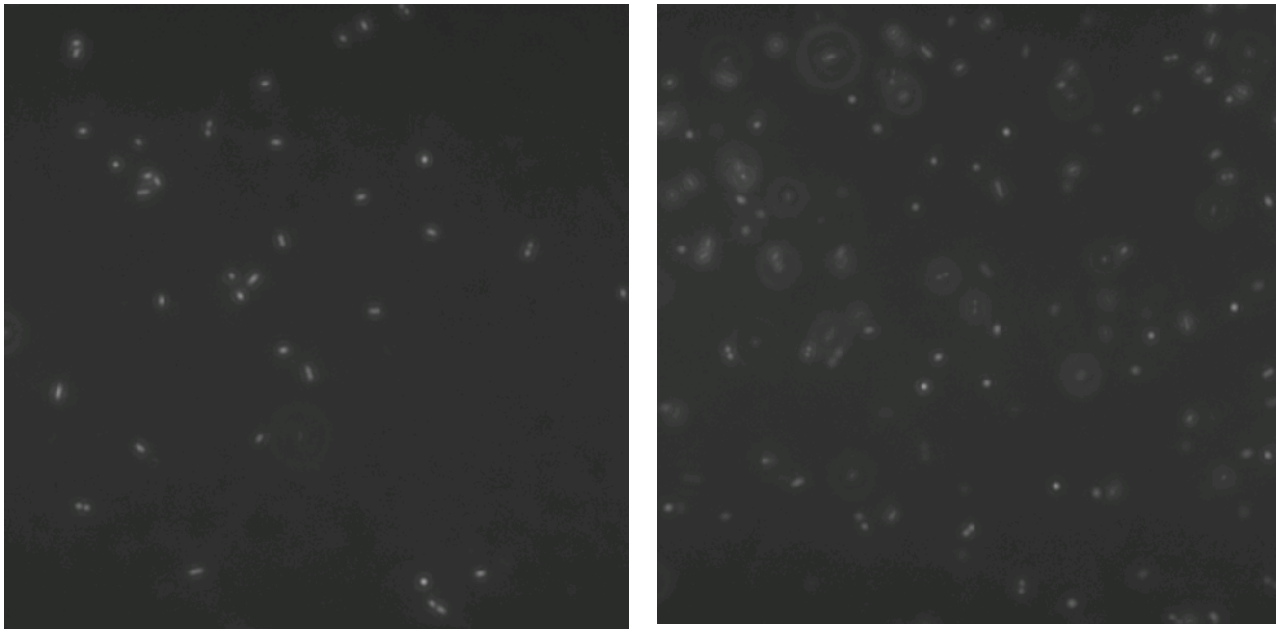

Figure 17 - Cell culture results on untreated (left) and treated (right) PETG

3.3. Surface energy

Additional samples were treated using a 3-Watt maximum Kr-F laser at Old Dominion University Applied Research Center in Newport News, Virginia. Because of the low power output of the laser, samples were surface treated for time periods ranging from 1 to 5 minutes at 1 Watt. This power delivered a continuous dose of 1.27 W / cm^2. Due to an internal malfunction within the laser that caused it to shut itself off if run at full power, 1 Watt was used instead of the laser's 3-Watt maximum. This was not considered to be an obstacle, as the extent of surface damage of the samples treated at 1000 mJ with the pulsed laser would not allow for accurate measurement of the surface energy through contact angles. Contact angle measurements were then taken using the two-liquid method for surface energy calculations [27]. Deionized water and CH_2I_2 were the two liquids chosen for this experiment.

As seen in Figure 18 below, there was little change apparent in the contact angle measurements as a function of dose. In the samples ablated at Virginia Tech,

undoubtedly there would be a significantly higher surface energy simply due to the extremely rough surface produced through treatment.

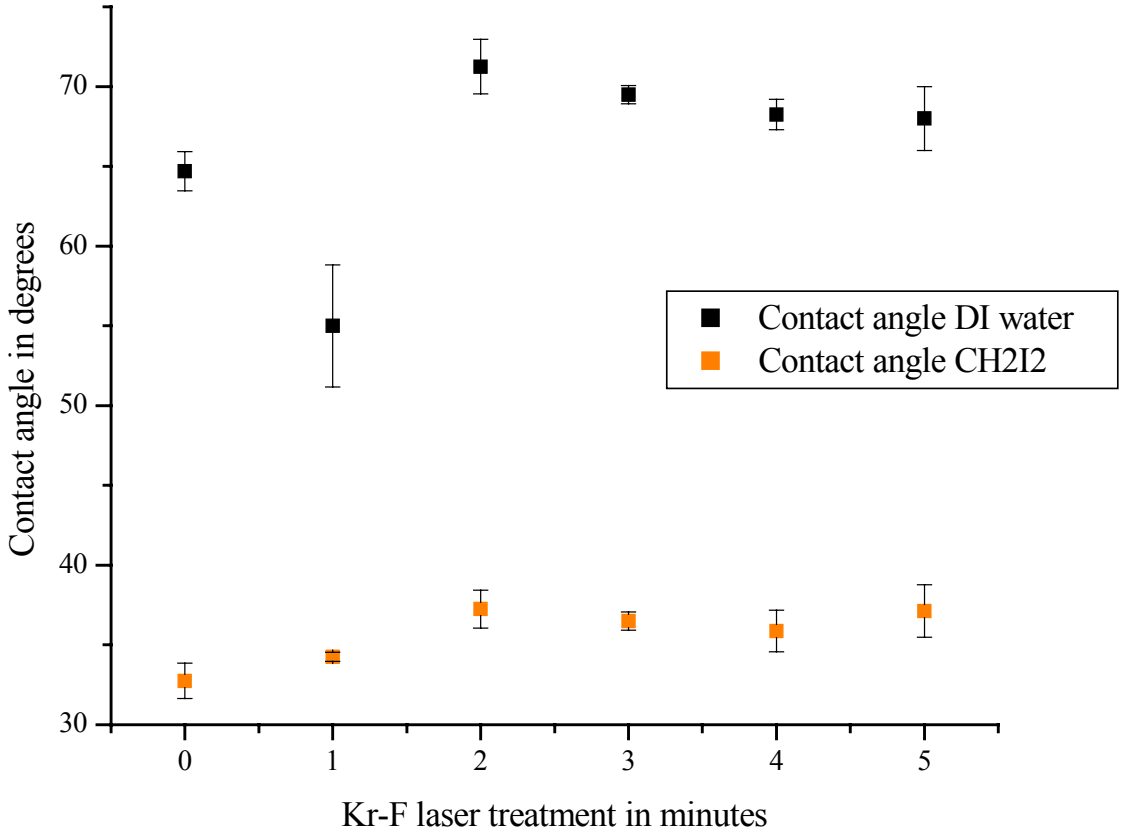

Figure 18 - Contact angle versus Kr-F laser treatment time for poly(methyl methacrylate)

PETG however, displayed a dose-dependent surface energy. This was expected based upon previous experiments that showed an increasingly hydrophilic surface with laser ablation of PETG [29]. However, what was unexpected was that the surface energy would return almost to its original value with increasing dose. Oddly, PTFE demonstrated a similarly parabolic correlation between dose and contact angle. The results of the contact angle experiments for PETG and PTFE are shown in Figure 19 and Figure 20 below.

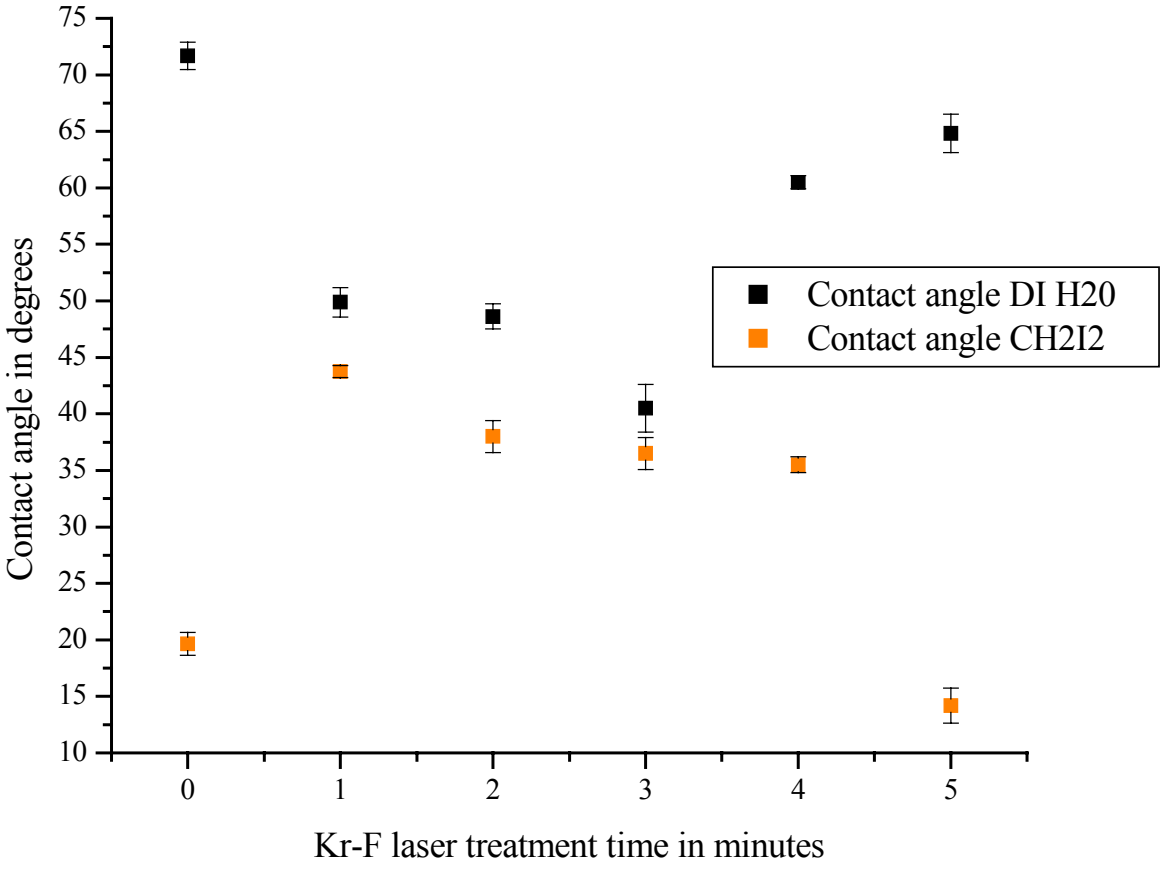

Figure 19 - Contact angle versus dose for glycol-treated poly(ethylene terephthalate)

The trend seen in the contact angle of treated PETG with water corresponds to the trends previously seen in PET treated with a Kr-F laser [29]. This study observed an immediate decrease in the contact angle, but with subsequent pulses, the contact angle returned to near its original value where it reached a steady state.

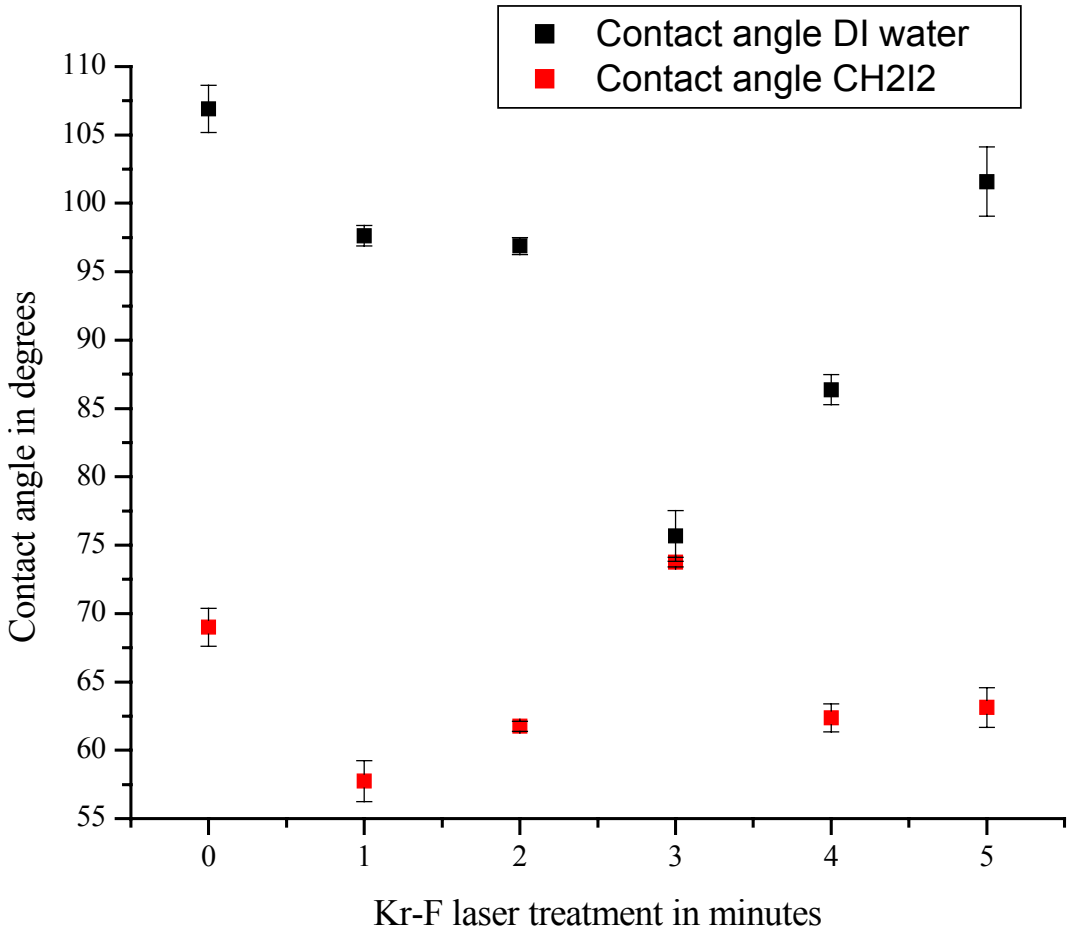

Figure 20 - Contact angle versus dose for polytetrafluoroethylene

Surface free energies for the three materials were calculated using a system of two equations and solving for the dispersive and polar components in Equation 5. The results of these surface energy calculations are shown in Figure 21 below.

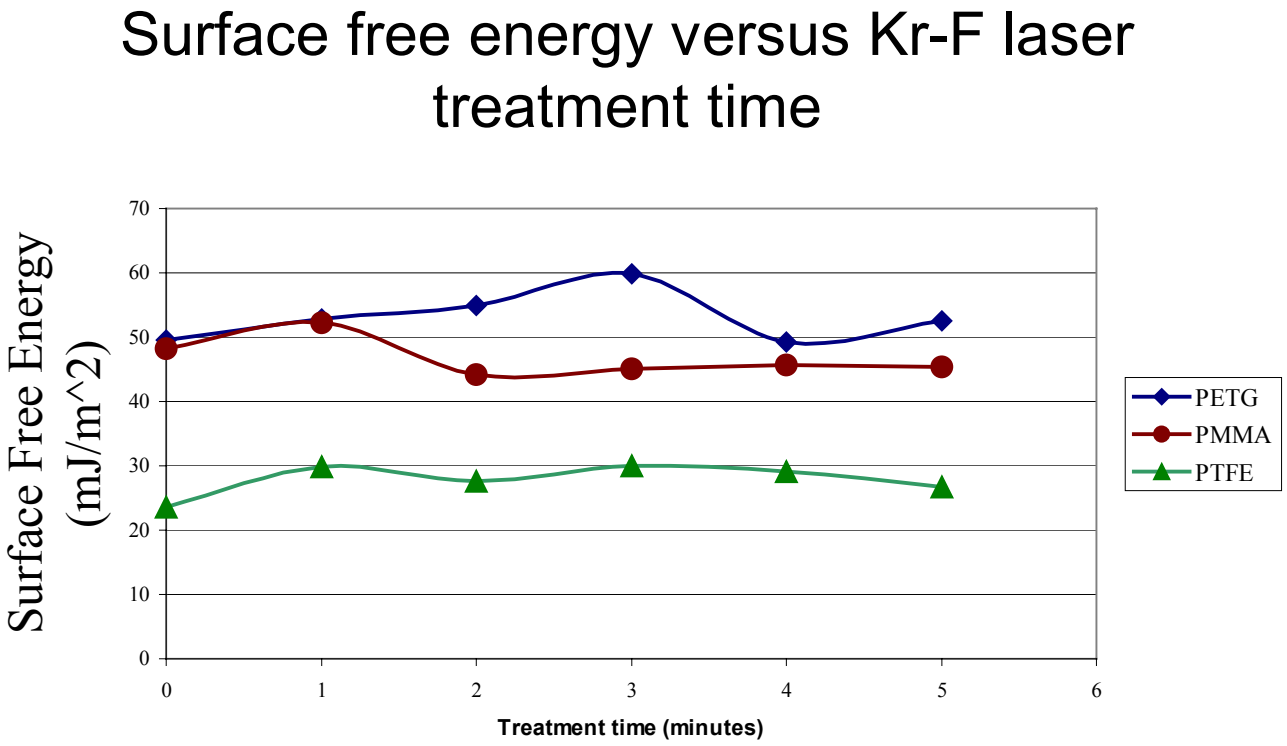

Figure 21 - Results of surface free energy calculations from contact angle measurements as a function of dose for PMMA, PETG, and PTFE

3.4. Surface composition

Surface compositional analysis was performed via x-ray photoelectron spectroscopy (XPS). An incident beam angle of 45° for untreated samples and 15° for treated samples was used. The glancing angle of 15° was used for the treated samples to ensure that only the surface composition was examined. XPS compositional analysis is derived from the plot of relative photoelectron density at the detector versus binding energy in electron volts. Each peak is characteristic to a bond or a set of bonds, so changes in the emission spectrum with treatment are an indication of bond cleavage with radiation exposure. The relevant peak assignments are shown in Table 7.

Table 7- XPS peak assigments for curve-fitted C1s photopeak

Peak position (ev)	Assignment
284.7	Aromatic
284.8	C=C
285.0	C-H, C-C
286.3-286.7	C-O
287.8-288.2	C=O
289.2	O=C-O
292.6	CF_2

The first material examined was poly(methyl methacrylate) (chemical structure shown below in Figure 22).

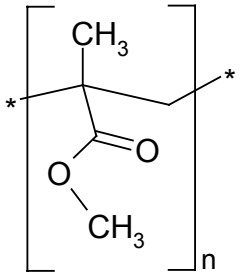

Figure 22 - Chemical structure of poly(methyl methacrylate)

In Figure 23, the survey scan of the untreated (top curve) and treated (bottom curve) polymethyl methacrylate, there appears to be little to no change in the surface chemistry of the polymer.

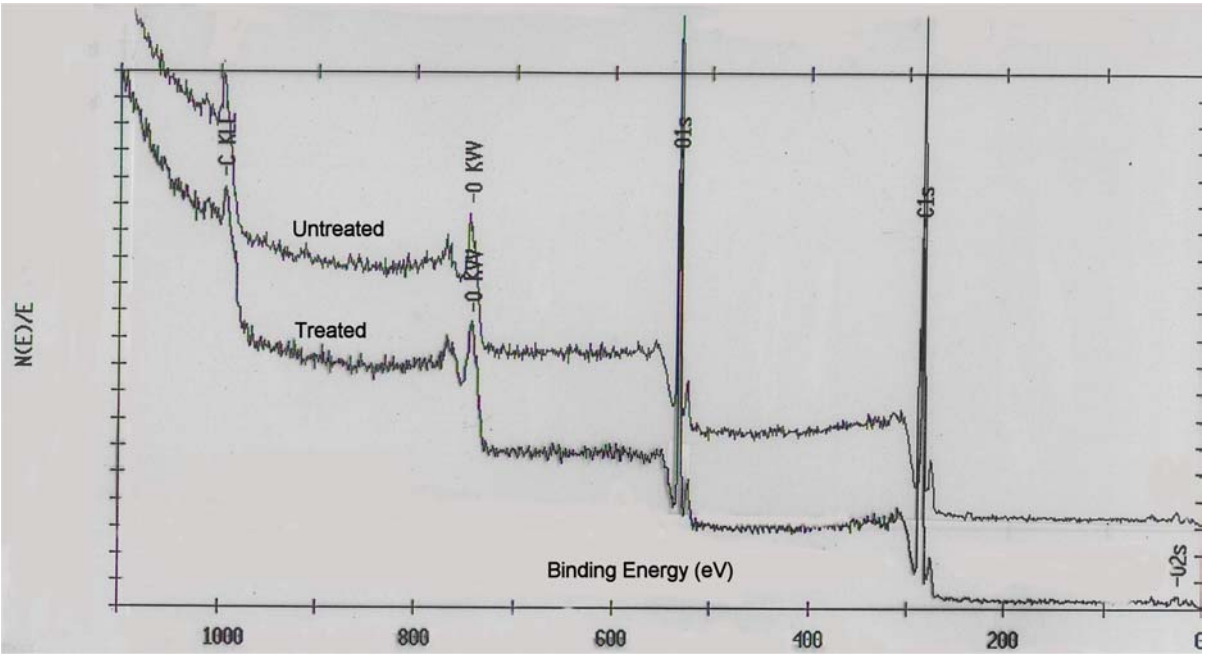

Figure 23 - XPS survey scan of treated and untreated poly(methyl methacrylate)

However, closer observation of the C1s and O1s peaks in the multiplex scans suggests otherwise. Notice in Figure 25, the multiplex scan of the C1s peak, there is an increase in the intensity corresponding to an increase in the C=O group. This suggests that there is cleavage in the ester group at the single-bonded oxygen.

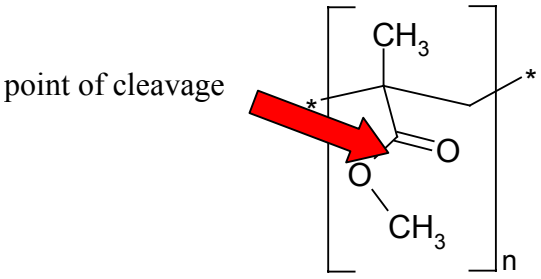

Figure 24 - Suggested mechanism of ablation for poly(methyl methacrylate)

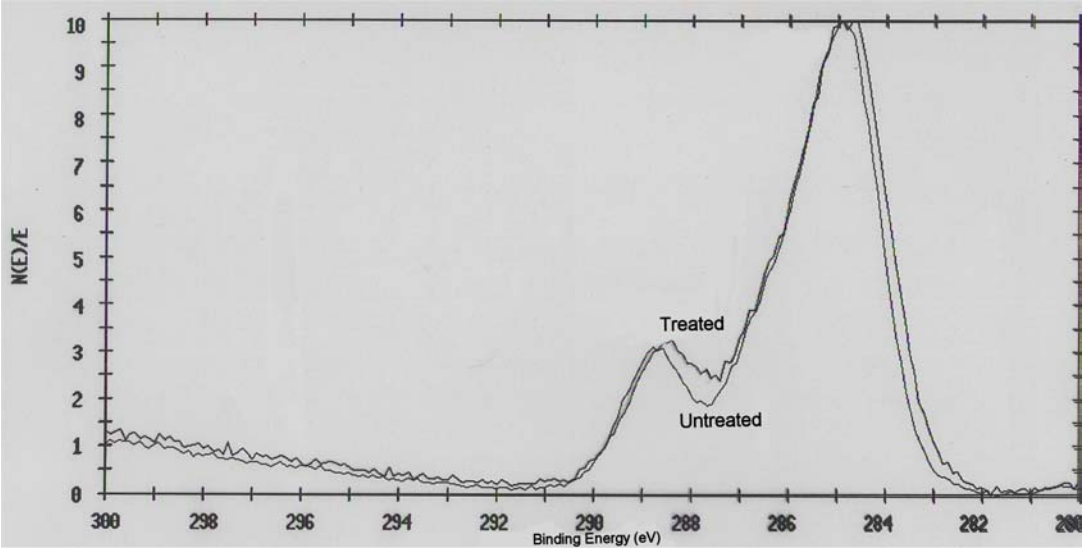

Figure 25 - XPS multiplex scan of the C1s region of both treated and untreated poly(methyl methacrylate)

The shift in the C1s region indicating and increase in C=O is further corroborated by the multiplex scan of the O1s region of PMMA shown in Figure 26. The narrowing and rightward shift of the O1s peak supports what was observed in the C1s region of PMMA.

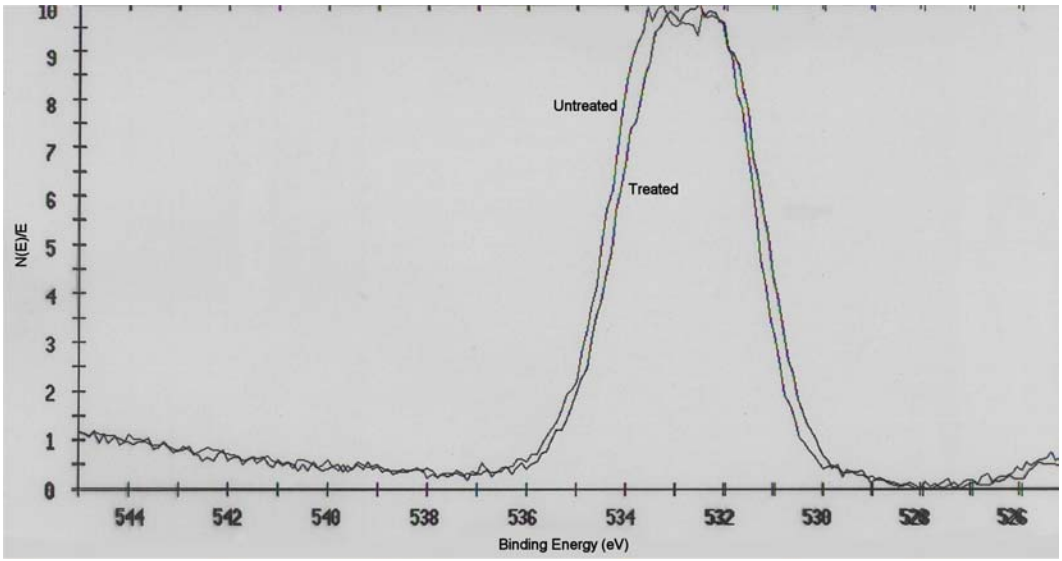

Figure 26 - XPS multiplex scan of the O1s region of both treated and untreated poly(methyl methacrylate)

The next material examined by XPS was polytetrafluoroethylene. Given the simplicity of the repeat structure of this polymer (see Figure 27), there should have only been two peaks, the C1s peak at 292.6 eV and the F1s peak at 690 eV. However, there were multiple peaks from 600 to 670 eV picked up in the survey scans of both the treated and untreated samples seen in Figure 28. These were confirmed to be secondary Auger peaks associated with fluorine that were identified as the F KLL transition in the work by Brewis [50, 51]. The fluorine 2S peak is also observable at 40 eV.

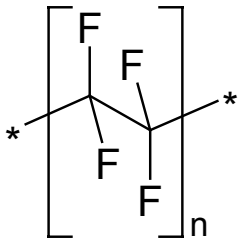

Figure 27 - Polytetrafluoroethylene chemical structure

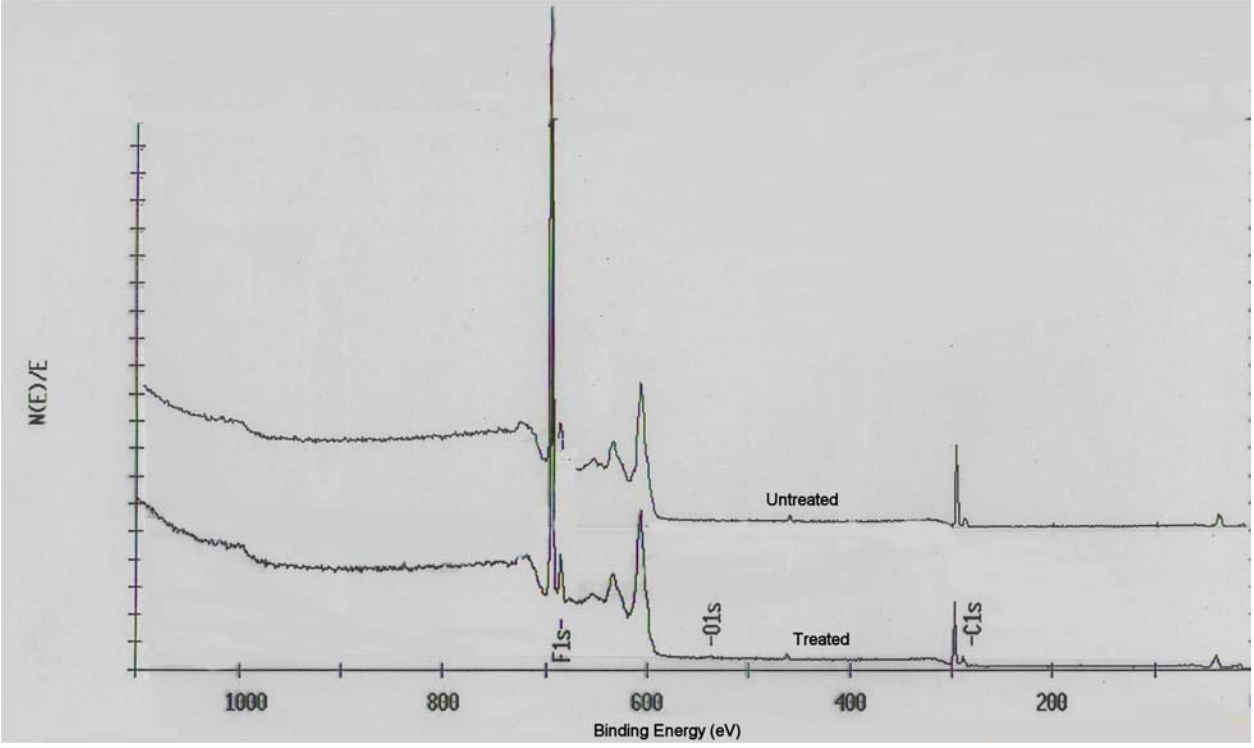

Figure 28 - XPS survey scan of both treated and untreated polytetrafluoroethylene

In the multiplex scan of the C1s region of PTFE (Figure 29), there is the sharp peak at 293 eV associated with CF_2 as expected. A smaller, broader peak at 285 eV was also observed. This peak is an indication of some level of hydrocarbon contaminant in the sample. The hydrocarbon peak intensity increased with laser treatment.

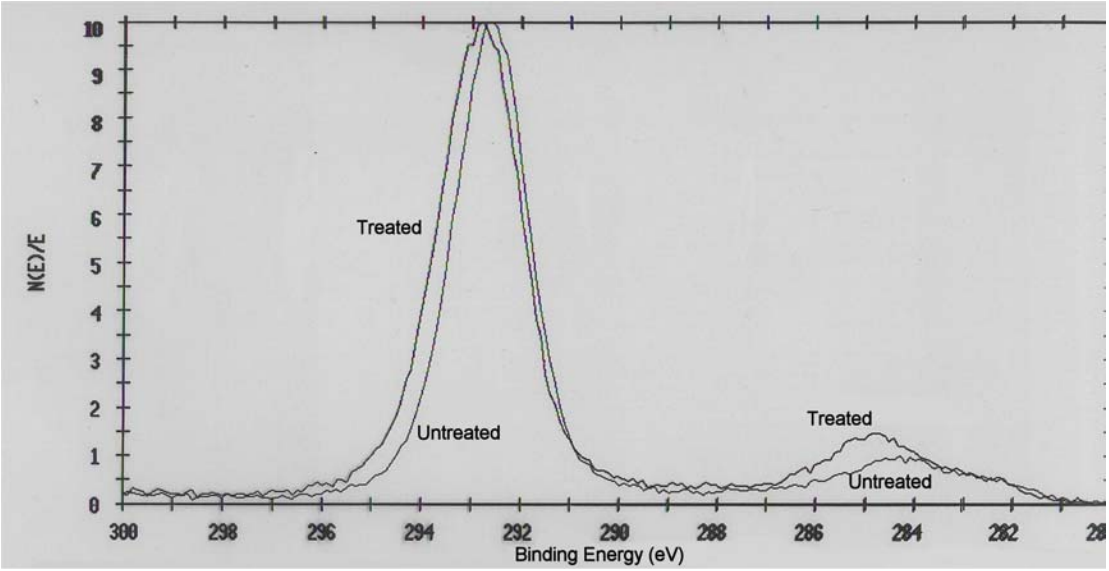

Figure 29 - XPS multiplex scan of C1s peak of treated and untreated polytetraflurorethylene

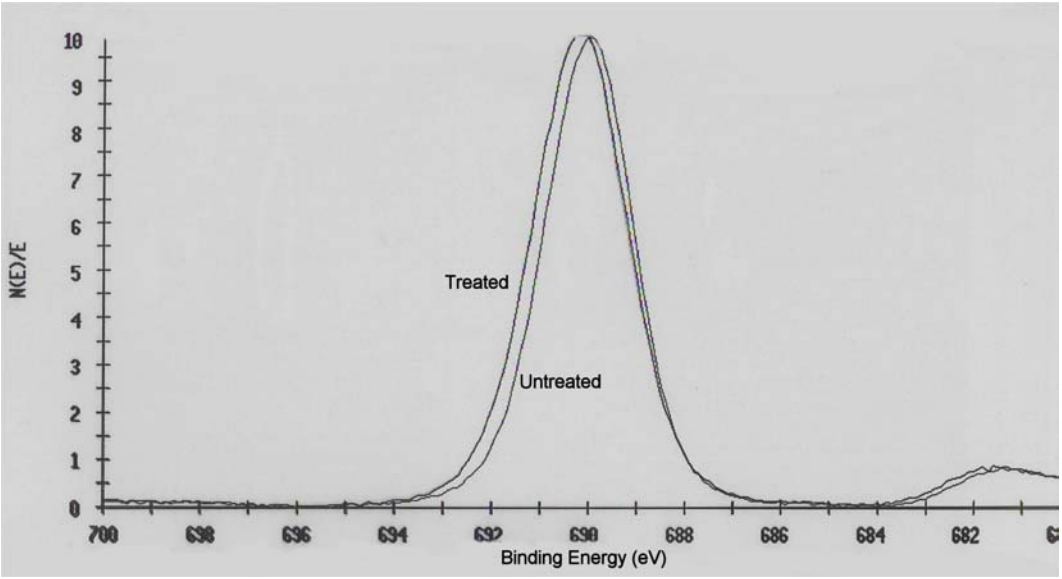

Figure 30 - XPS multiplex scan of F1s region of both treated and untreated polytetrafluoroethylene

The final material examined for surface composition was glycol-treated polyethylene terephthalate (PETG). This particular material is a terpolymer composed of the three molecules shown below. This means that every other molecule in the chain is 1,4 – Benzenedicarboxylic acid, or dimethyl terephthalate and every other molecule is either ethylene glycol or 1,4 – cyclohexanedimethanol. The structures of the three constituent molecules are shown in Figure 31 below.

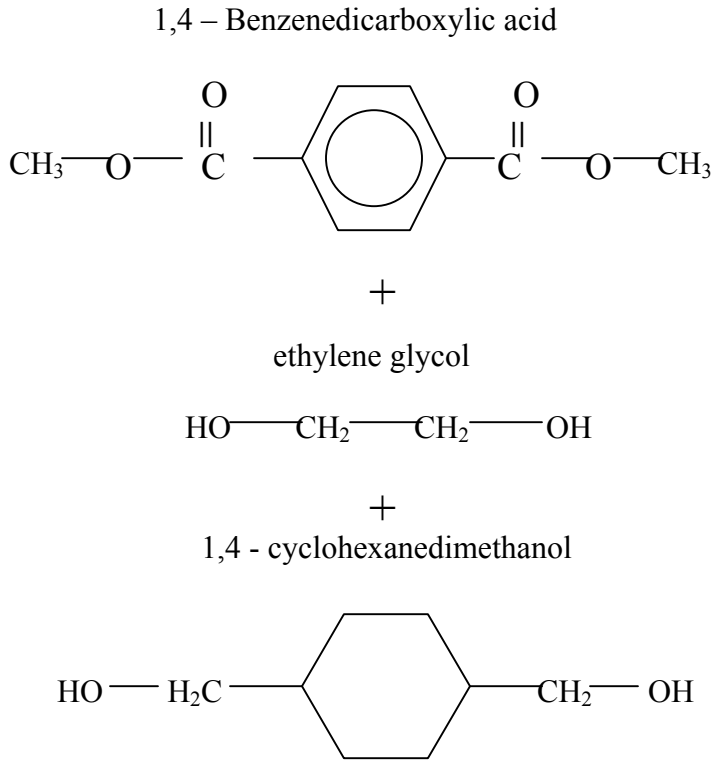

Figure 31 - Chemical structure of glycol-treated poly(ethylene terephthalate)

As in the case of PMMA, there was evidence in PETG (C1s region shown in Figure 32) of an increase in the relative number of C=O groups (288 eV) that corresponded to a decrease in the relative number of O-C=O groups (289.2 eV). This could be an indication of the point of cleavage of the chain and would be a point where cleavage would be expected. Also notice in Figure 34 the decreased width of the oxygen peak corresponding to the decrease in the relative oxygen content. Finally, there was some

nitrogen contamination introduced with laser treatment indicated in the survey scan in Figure 33 at 400 eV.

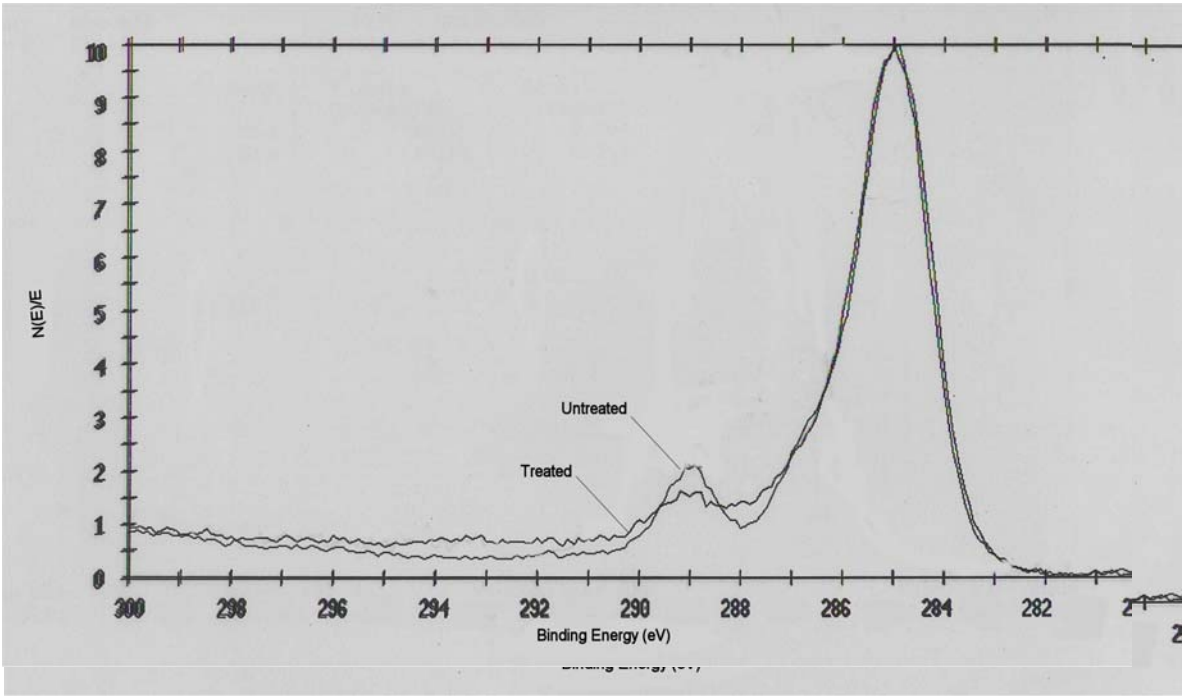

Figure 32 - XPS of C1s region of glycol-treated poly(ethylene terephthalate)

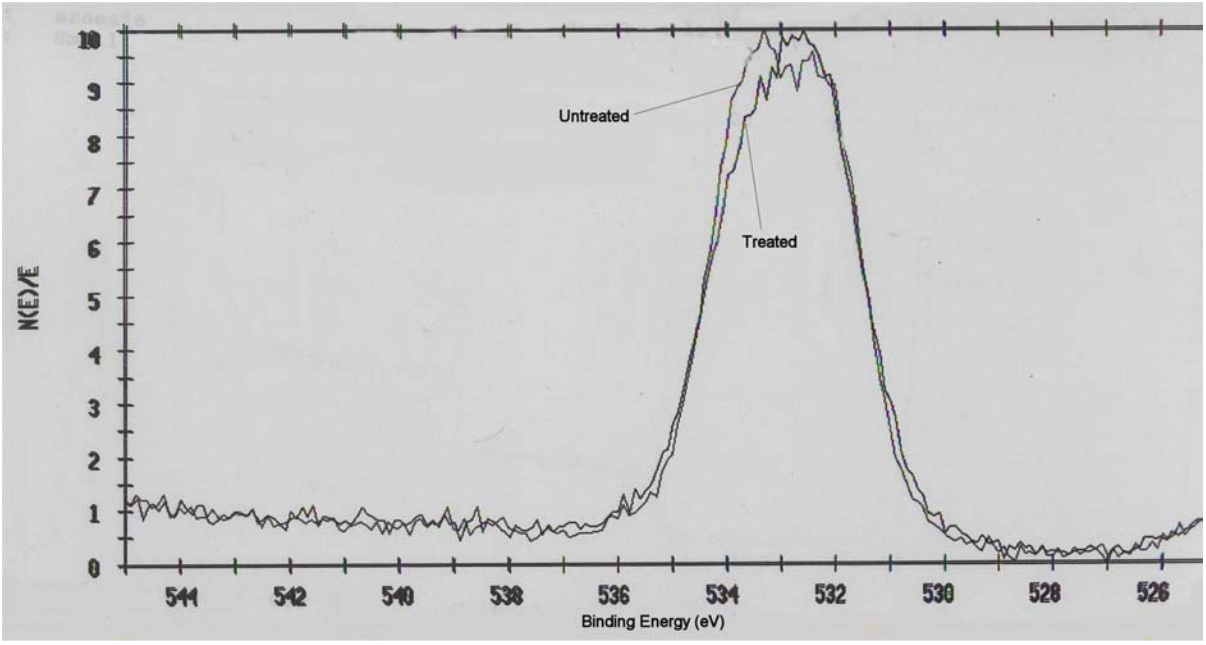

Figure 33 - XPS of O1s region of glycol-treated poly(ethylene terephthalate)

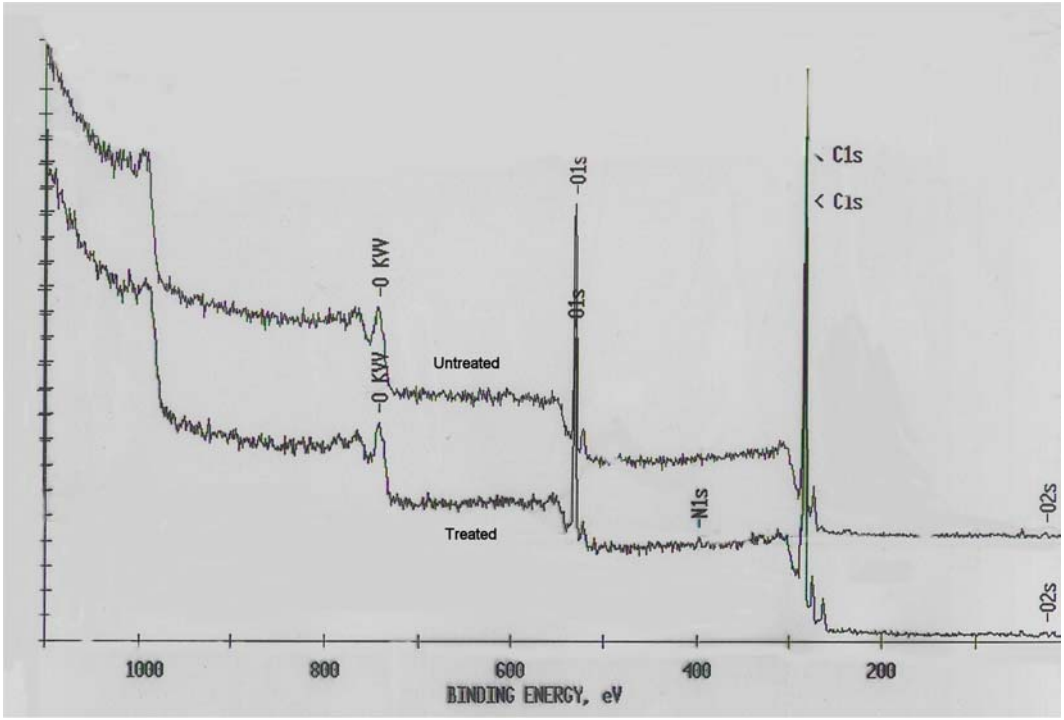

Figure 34 - XPS multiplex scan of glycol-treated polyethylene terephthalate

Through calculation of relative peak areas, XPS can determine percent composition of the sample surface. A summary of the percent composition of the treated and untreated specimens can be seen below in Table 8.

Table 8 - Relative percent concentration of elements as determined by XPS

Element	**PMMA untreated**	**PMMA treated**	**PTFE untreated**	**PTFE treated**	**PETG untreated**	**PETG treated**
C1s	74.7	74.5	37.1	37.6	79.3	80.7
O1s	25.3	25.5		0.5	20.7	18.2
F1s			62.9	62.0		
N1s						1.2

3.5. Surface topography

Samples were observed by optical microscopy as well as a scanning electron microscope at several different magnifications to determine changes in surface topography. Poly(methyl methacrylate) showed the most significant modification of surface structure of the three materials.

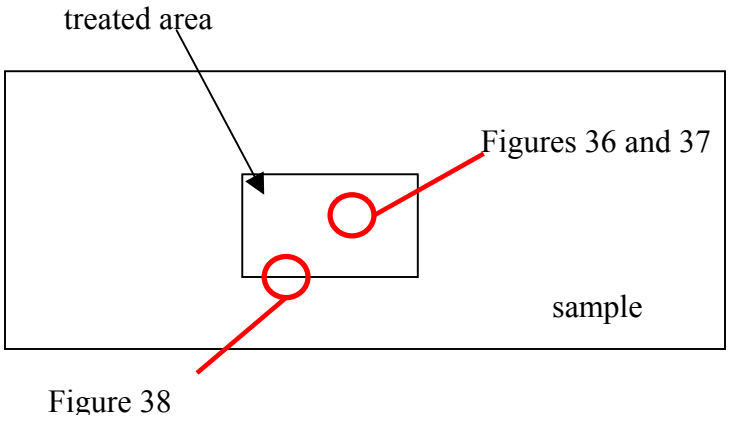

Figure 35 - Schematic of microscopy areas for Figures 36 through 38

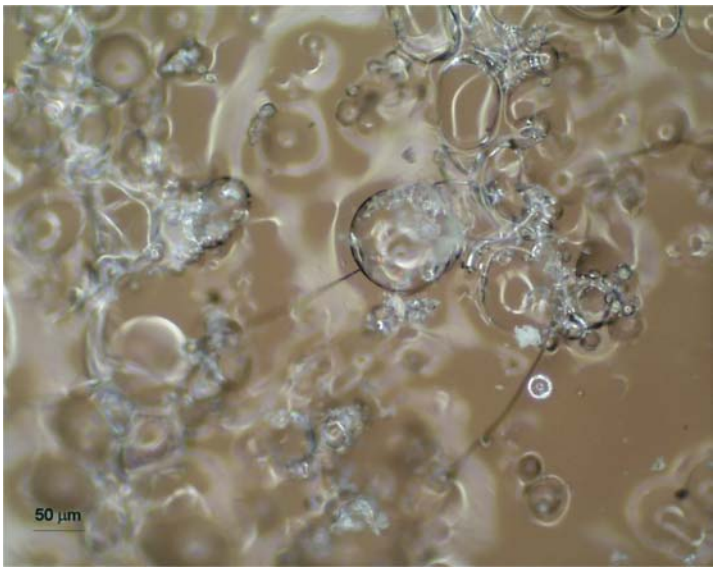

Figure 36 – Micrograph of the center of the ablated PMMA surface

As illustrated in Figure 36, laser treatment of PMMA produced a bubbling effect that resulted in a crater-like structure. This effect is thought to be a result of sub-surface superheating. There is also evidence of crack propagation due to thermal stresses incurred during the superheating event.

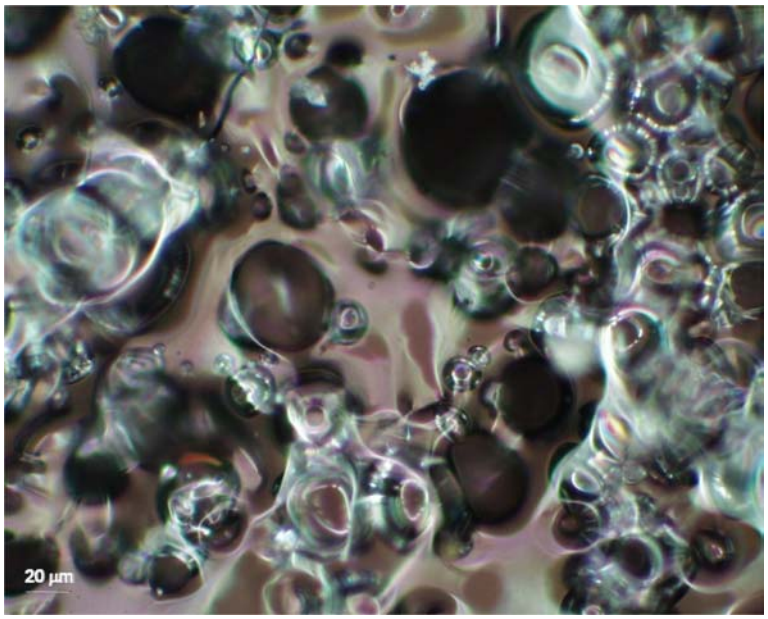

Figure 37 – Micrograph of the center of the ablated poly(methyl methacrylate) area

Upon further observation, it became evident that the bubbled structure was not only on, but somewhat below the surface as well. Bubbles ranged in size from 5 µm to 50 µm and covered the majority of the treated surface.

The micrograph of the edge of the treated PMMA sample shown in Figure 38 shows a definitive difference between the smooth untreated surface on the right and the treated area on the left. Notice however the debris deposited on the untreated surface by ablation. Scanning electron microscopy of the PMMA surface shows the details of the ablation process more completely.

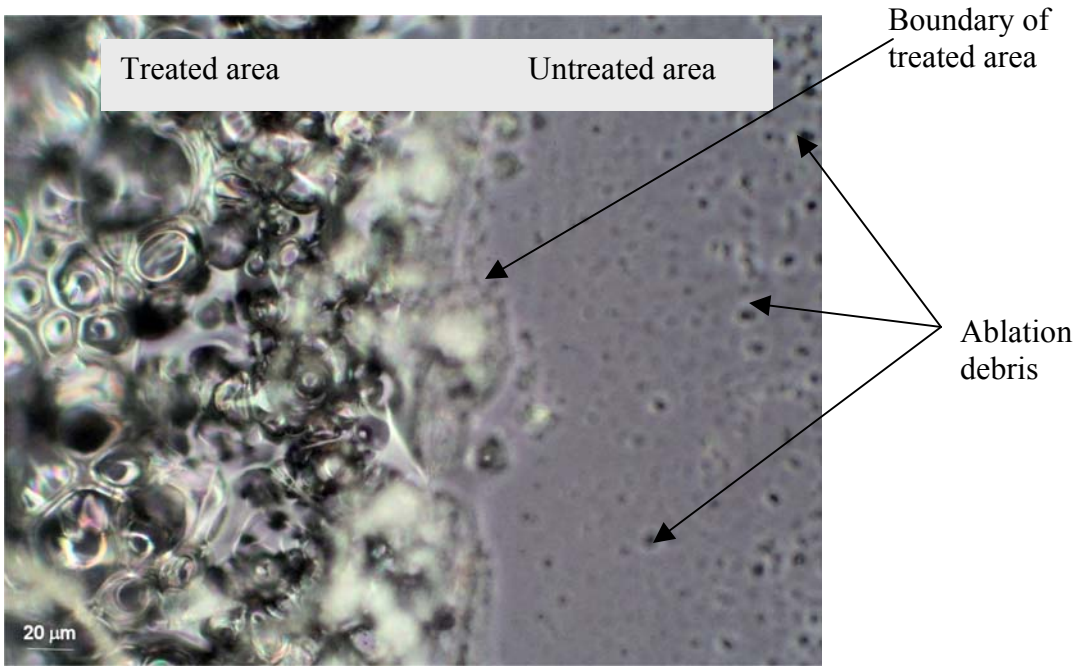

Figure 38 – Micrograph of PMMA sample at the boundary of the treated area

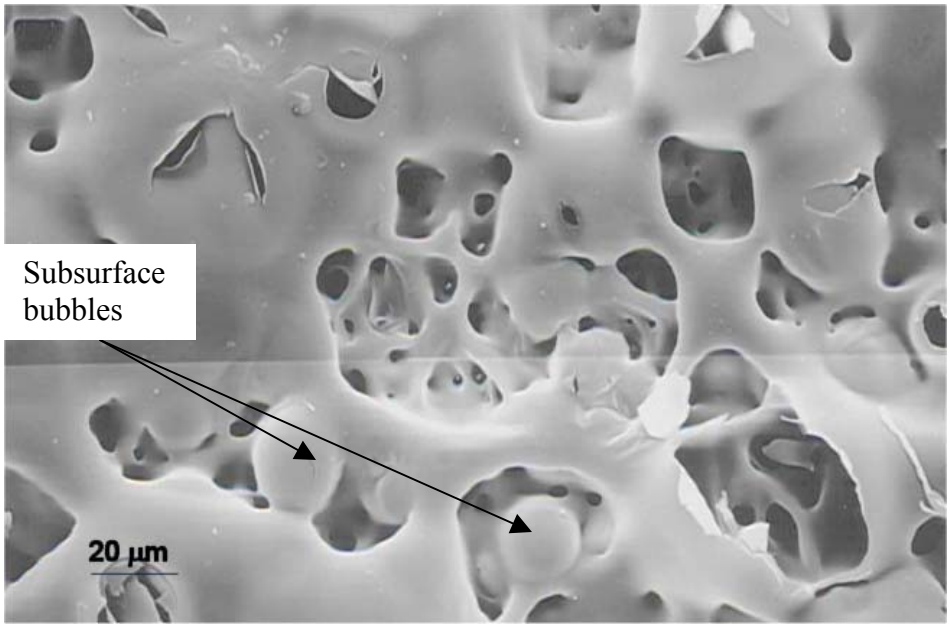

Figure 39 - SEM of poly(methyl methacrylate) surface ablated at 1000 mJ for 20 pulses

From the scanning electron micrograph shown in Figure 39, the development of subsurface microbubbles can be observed. These bubbles subsequently rise to the surface and burst, resulting in a cratered structure and the formation of debris.

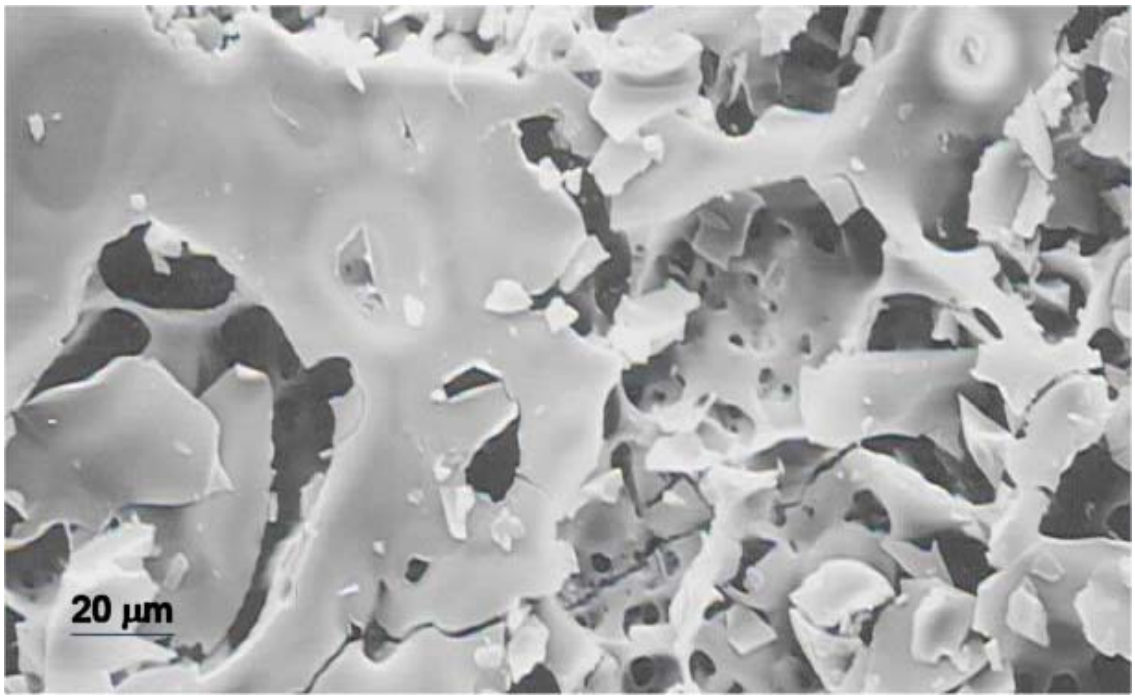

Figure 40 - SEM of PMMA surface ablated at 1000 mJ for 20 pulses

Figure 40 shows another portion of the ablated PMMA surface in an area of the sample where more bubbles have burst, leaving behind PMMA fragments. Thermally induced cracking of the surface can also be observed in this sample, similar to that seen using optical microscopy in Figure 36.

When the ablated PMMA surface is observed at a slightly lower magnification as is the case in Figure 41, the extent of surface damage due to the laser treatment becomes more readily apparent; the entire surface appears to be affected. The extent of, as well as mode of destruction appears to be different in the case of polytetrafluoroethylene, as seen in Figure 42.

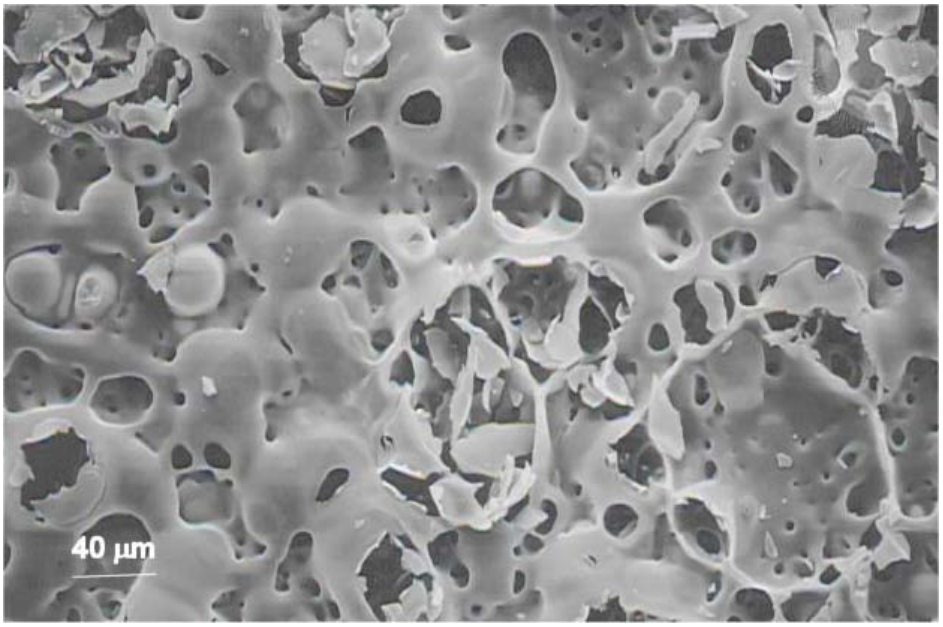

Figure 41 – SEM of PMMA surface ablated at 1000 mJ and 20 pulses

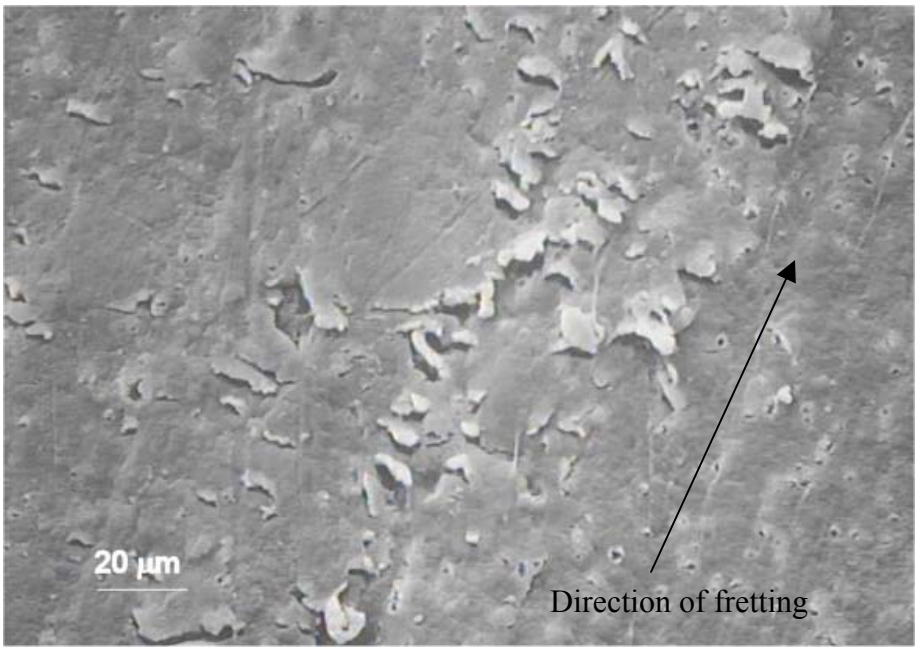

Figure 42 - SEM of PTFE surface ablated at 1000 mJ for 1 pulse

As shown in Figure 42, even with only one laser pulse, the surface begins to fret away along the striations left in the surface by processing. This can be seen in a greater extent at a slightly lower magnification as in Figure 43 below. Notice the directionality of the ablation process, much different than in the case of PMMA, where the entire surface began uniformly superheating.

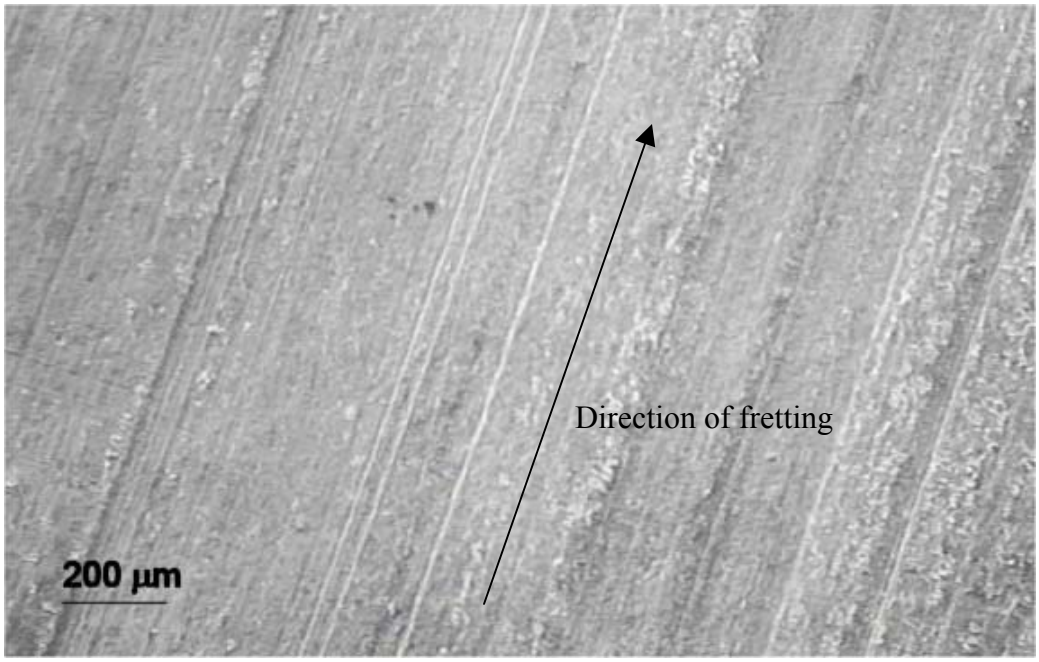

Figure 43 - SEM of polytetrafluoroethylene surface ablated at 1000 mJ for 1 pulse

Subsequent doses of radiation simply amplified this effect further. Notice in Figure 44 that the fretting of the surface material continues to be directional, even at this high level of damage.

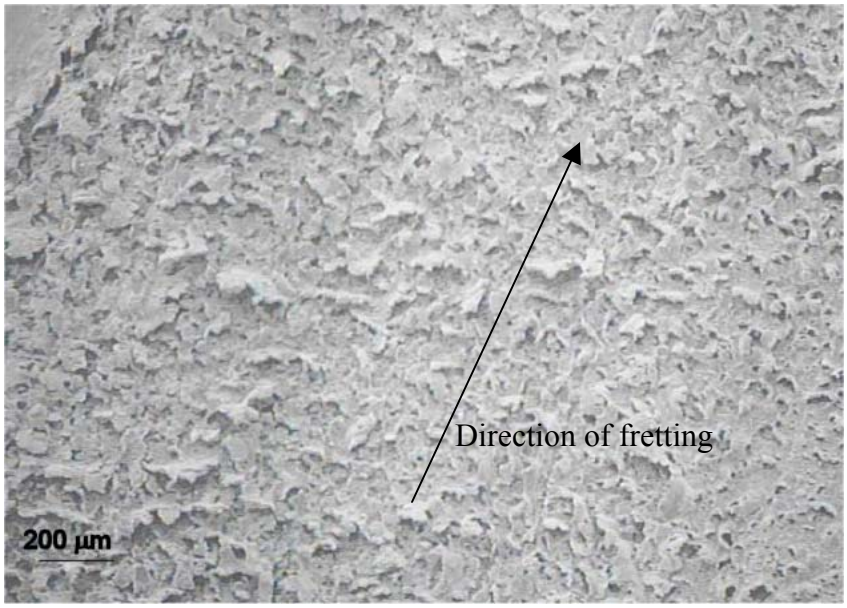

Figure 44 - SEM of polytetrafluoroethylene surface ablated at 1000 mJ for 20 pulses

The resulting surface structure is very rough and flaked (see Figure 45), with little to no loose surface debris. Such a surface should be ideal to promote cellular attachment by mechanical means.

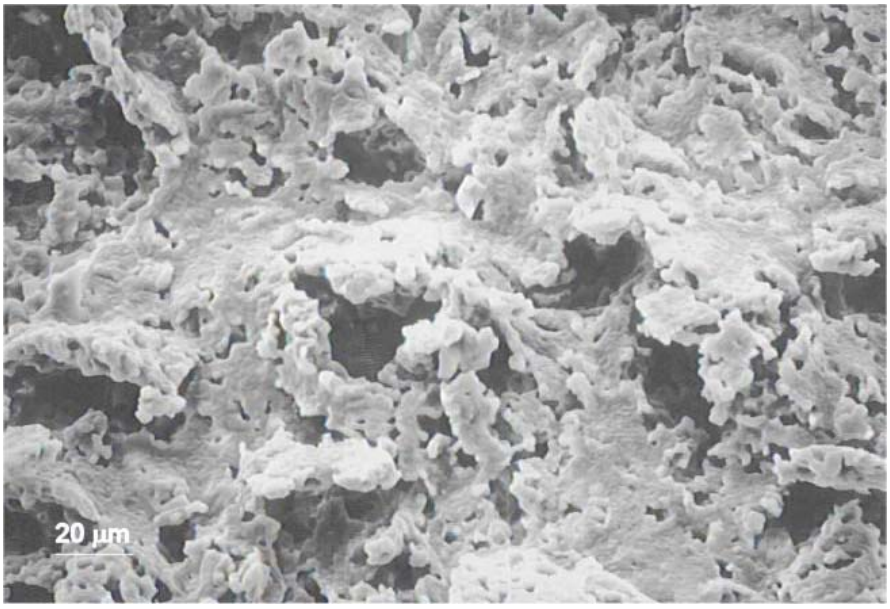

Figure 45 - SEM of polytetrafluoroethylene surface ablated at 1000 mJ for 20 pulses

The charring around the edged of the ablated PTFE area is observed by optical microscopy in Figure 46 as embedded burnt particulates in the surface, indicating that indeed there is some debris coming off the surface in conjunction with the ablation process.

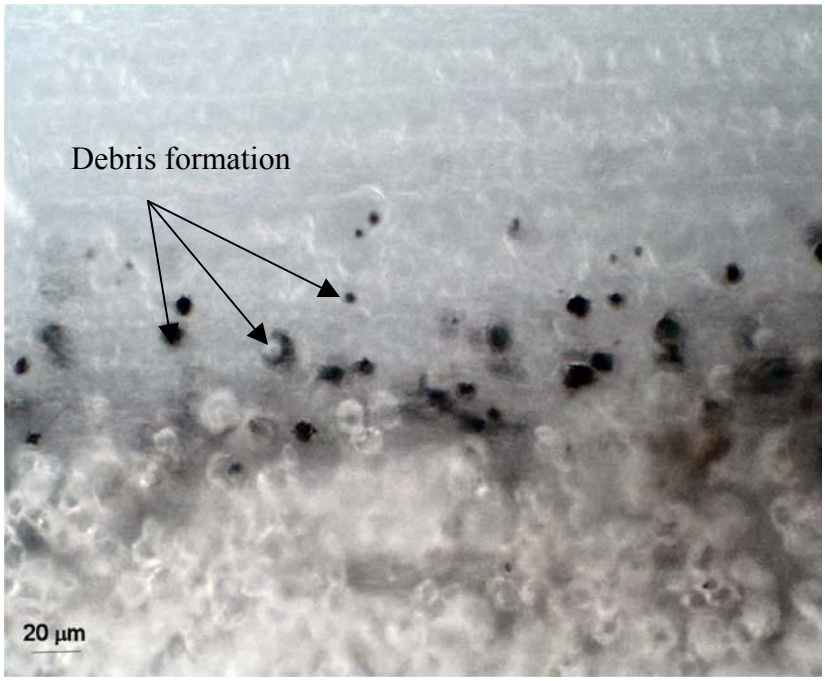

Figure 46 - Micrograph of the boundary of the polytetrafluoroethylene ablated area

Surface texture of treated PMMA and PTFE was characterized using the scanning electron micrographs presented in Figures 36-46. Frequency distributions of the feature sizes present following laser treatment were determined and are presented in Figure 47 below. Notice the frequency of occurrence of the less than 5 μm features in these two materials. PTFE ablated through a fretting mechanism by which cracks were initiated along crystal boundaries, then propagated until material was removed. These cracks make up the majority of the less than 5 μm features. In the case of PMMA, where ablation occurred through subsurface superheating and resulting bubble formation, the nucleation size defined the feature size on the material surface. The smallest pores

observed were approximately 5 μm. It is believed that the smaller gaseous bubbles may aggregate and form large bubbles which then surface to create the large features observed. The less than 5 micron features observed within these larger pores seem consistent with gas bubbles that did not aggregate. It would be interesting to study the pore size as a function of radiation dose for PMMA to see if the aggregation of gases is dose-dependent.

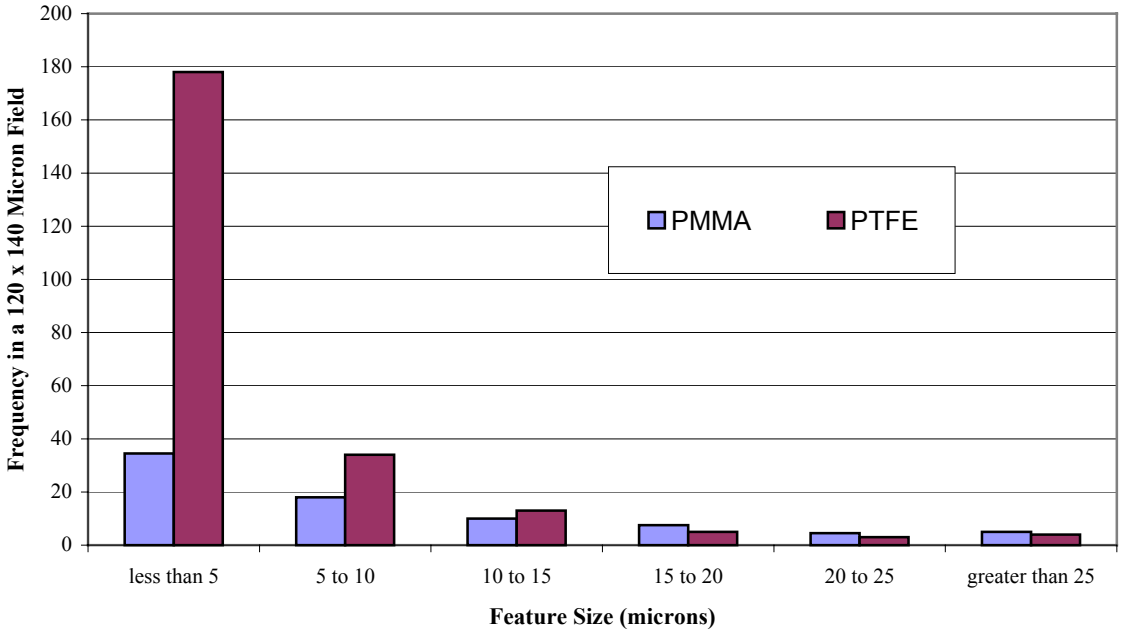

Figure 47 - Feature size distribution for PMMA and PTFE treated at 1000 mJ for 20 pulses of Kr-F laser radiation

In contrast to both PMMA and PTFE, PETG showed little to no signs of enhanced surface roughness with ablation. While there appears to be some surface texture as seen in Figure 48, it is nothing like the bubbling or fretting effects seen in the other two materials.

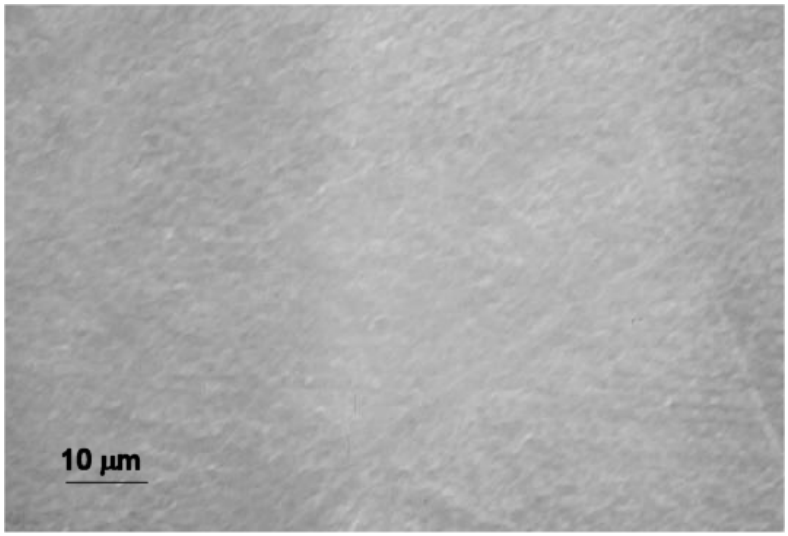

Figure 48 - SEM of PETG surface ablated at 1000 mJ for 20 pulses

To ensure that ablation was actually occurring, a PETG sample was observed using optical microscopy in reflectance with a polarizing filter. Inspection of the edge of the treated area shown in Figure 49 revealed that material was indeed being removed from the surface.

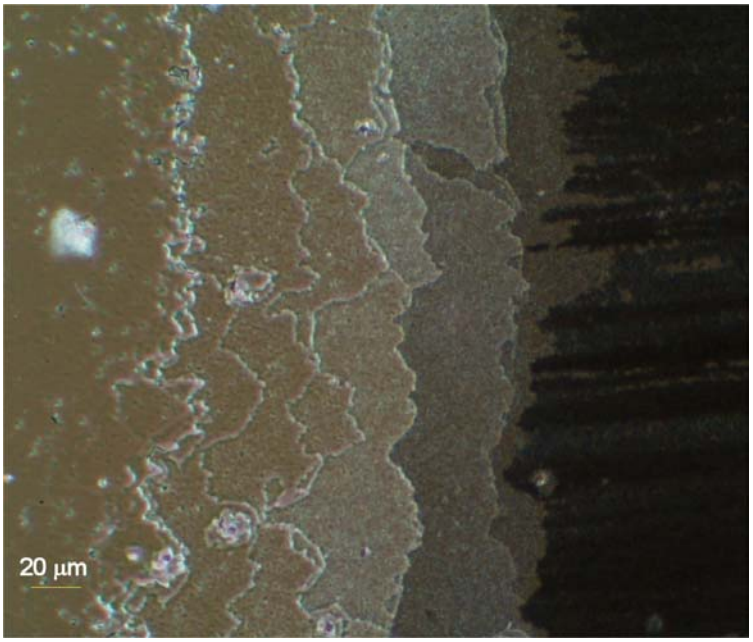

Figure 49 - Micrograph of edge of PETG ablated surface

Further observation showed the formation of crystallites in the ablation region in a material that is manufactured to maintain an amorphous structure. The formation of these crystallites indicates that perhaps the additive that is supposed to retain the amorphous nature of this polyester is eluding during ablation. Examples of the crystallite formation are shown in Figures 50 and 51.

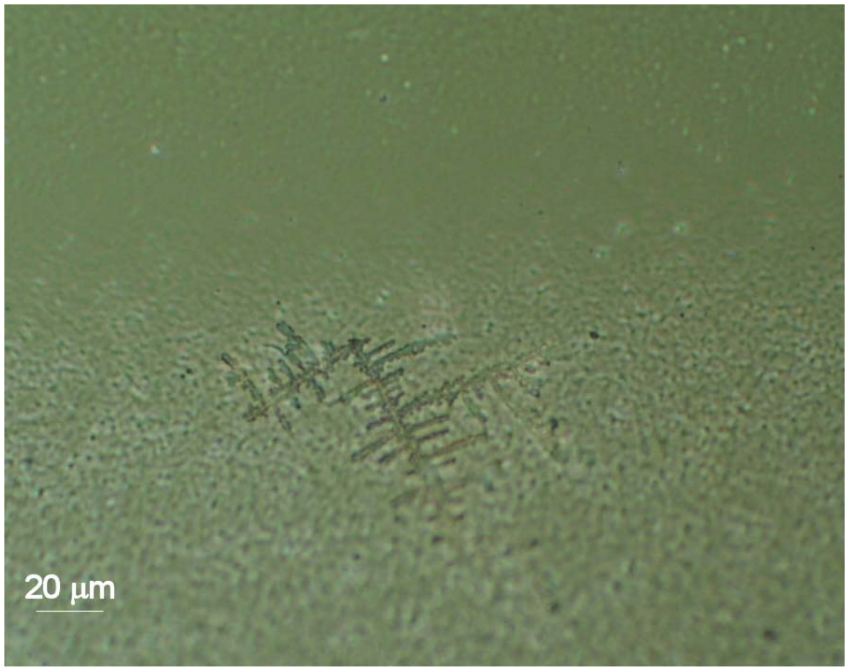

Figure 50 - Micrograph of crystallite on PETG ablated surface

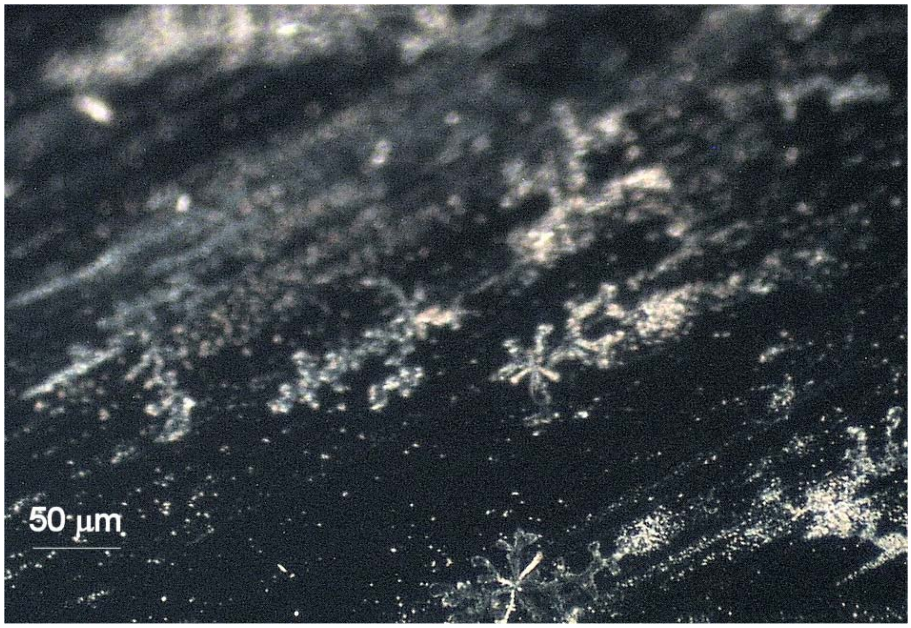

Figure 51 - Micrograph of crystallites on ablated PETG surface

It is interesting to notice that the two substrates that were visibly roughened with laser surface treatment, PMMA and PTFE, showed poorer cell adhesion than unmodified, smooth samples. The treatment also significantly improved adhesion to PETG, a substrate that showed few visible signs of surface roughening. These results are contrary to the theory of cell adhesion by mechanical means, indicating that the change in cellular attachment is due to surface chemistry or surface free energy effects. This idea will be further described in Section 4.

4. Conclusions

This work examined the effect Kr-F laser irradiation had on three polymer substrates: PMMA, PTFE, and PETG and attempted to correlate the surface modifications in topography, surface chemistry, and surface free energy to the polymers' bacterial adhesion properties. Laser ablation induced some surface topographical changes in all three polymers. These changes were very subtle in PETG and therefore difficult to image, but there was some evidence of an induced rolling structure as described in the introductory section to this work. However, it appears that the

combination of mild surface roughness changes combined with slight modifications in the surface chemistry and surface free energy were sufficient to enhance bacterial attachment. The changes in surface roughness were not as subtle in PMMA and PTFE. The PMMA surface became cratered as gases were released from superheated subsurface material. There was evidence of preferential bacterial attachment in these cratered areas. However, it appears that the presence of surface roughness in these two materials could not overcome surface chemistry and surface free energy effects that served to sufficiently deter bacterial attachment. Through this work, it becomes apparent that it is crucial to strike the right balance of surface chemistry, surface free energy, and surface roughness to enhance bacterial attachment. From the work of van Loosdrecht et al [25], it is also apparent that where that balance of surface properties lies is dependent on the cell being investigated.

5. Future Work

In the future, it would be interesting to investigate further the correlation between radiation dose and contact angle. By then performing cell culture experiments on samples with various levels of surface modification (unlike the binary experiment performed in this work), perhaps the factors affecting bacterial adhesion could be better identified.

6. References

1. Ikada, Y. (1994). "Surface modification of polymers for medical applications." Biomaterials 15(10): 725-736.
2. Efthimiopoulos T, K. C., Heliotis G, Heliodonis E (2000). "Evidence of volume bubble creation during laser ablation of PMMA organic polymer." Canadian Journal of Physics 78: 509-519.
3. Dadsetan M, M. H., Sharifi-Sanjani N, Daliri M (2001). "Cell behavior on laser surface-modified polyethylene terephthalate in vitro." Journal of Biomedical Materials Research 57: 183-189.

4. Wefers L, S. E. (1993). "Surface characterization of laser-treated poly(ethylene terephthalate by optical profilometry and scanning tunneling microscopy." Journal of Polymer Science B 31: 23-27.
5. Hopp B, C. M., Revesz K, Vinko J, Bor Z (1996). "Formation of the surface structure of polyethylene-terephthalate (PET) due to ArF excimer laser ablation." Applied Surface Science 96-68: 611-616.
6. Hunt, J. A. a. D. F. W. (1995). "Quantifying the soft tissue response to implanted materials." Biomaterials 16(3): 167-170.
7. Swain GW, N. W., Preedeekanit S (1998). "The influence of biofouling adhesion and biotic disturbamce on the development of fouling communities on non-toxic surfaces." Biofouling 12(1-3): 257-269.
8. Suggs LJ, M. S., CA Garcia, JM Anderson, AG Mikos (1999). "In vitro cytotoxicity and in vivo biocompatibility of poly(propylene fumarate-co-ethylene glycol) hydrogels." Journal of Biomedical Materials Research 46: 22-32.
9. Peltola T, P. H., Moritz N, Areva S, Korventausta J, Jokinen M, Narhi T, Happonen RP, and Yli-urpo A (2002). "Methods to enhance biomimetic activity and ability to tissue bonding of sol-gel-derived nanoporous titania." Key Engineering Materials 218-220: 207-212.
10. Wimmer, R. (2001). "Development of an upset early warning device (UEWD) to predict defloculation effects." Unpublished.
11. Cote MF, D. C. (1992). "Wettability of cross-linked collagenous biomaterials: in vitro study." Biomaterials 13(9): 612-616.
12. DeFife KM, C. E., Nakayama Y, Matsudy T, Anderson JM (1999). "Spatial regulation and surface chemistry control of monocyte/macrophage adhesion and foreign body giant cell formation by photochemically micropatterned surfaces." Journal of Biomedical Materials Research 45: 148-154.
13. Dewez J-L, L. J.-B., Detrain E, Berger V, Dupont-Gillian CC, Vincent LM, Schneider Y-J, Bertrand P, Rouxhet PG (1998). "Adhesion of mammalian cells to polymer surfaces: from physical chemistry of surfaces to selective adhesion on defined patterns." Biomaterials 19: 1441-1445.

14. Gallardo-Moreno AM, G.-M. M., Bruque JM, Perez-Giraldo C, Gomez-Garcia AC (2002). "Temperature influence on the physicochemical surface properties and adhesion behaviour of Enterococcus faecalis to glass and silicone." Journal of Adhesion Science and Technology 16(9): 1215-1223.
15. Graham PD, J. I., Nevell TG, Smith JR, Stone M, and Tsibouklis J (2000). "Bacterial colonisation and settlement of algal spores and barnacle larvae on low surface energy materials." Biofouling 16(2-4): 289+.
16. Horbett TA, W. J., Ratner BD, Hoffman AS (1988). "Cell adhesion to s series of hydrophilic-hydrophobic copolymers studied with a spinning disc apparatus." Journal of Biomedical Materials Research 22: 383-404.
17. Jenney CR, A. J. (1999). "Effects of surface-coupled polyethylene oxide on human macrophage adhesion and foreign body giant cell formation in vitro." Journal of Biomedical Materials Research 44: 206-216.
18. Lee JH, P. J., Lee HB (1991). "Cell adhesion and growth on polymer surfaces with hydroxyl groups prepared by water vapour plasma treatment." Biomaterials 12: 443-448.
19. Matsuda T, C. D.-J. (1994). "Microfabricated surface designs for cell culture and diagnosis." ASAIO Journal 40: M594-M597.
20. Meylheue T, v. O. C., Bellon-Fontaine MN (2001). "Adsorption of biosurfactant on solid surfaces and consequences regarding the bioadhesion of Listeria monocytogenes LO28." Journal of Applied Microbiology 91(5): 822-832.
21. Mirzadeh H, K. A., Khorasani, Burford RP, Gorgin E, Golestani A (1995). "Cell attachment to laser-induced AAm- and HEMA-grafted ethylene-porpylene rubber as biomaterial: in vivo study." Biomaterials 16(8): 641-648.
22. Picioreanu C, v. L. M., Heijnen JJ (2000). "Two-dimensional model of biofilm detatchment caused by internal stress from liquid flow." Biotechnology and Bioengineering 72(2): 205-218.
23. Schankenraad JM, B. H., Wildevuur CRH, Arends J (1986). "The influence of substratum surface free energy on growth and spreading of human fibroblasts in the presence and absence of sefum proteins." Journal of Biomedical Materials Research 20: 773-784.

24. Steele JG, D. B., Johnsom G, Underwood PA (1993). "Polystyrene chemistry affects vitronectin activity: an explaination for cell attachment to tissue culture polystyrene but not to unmodified polystyrene." Journal of Biomedical Materials Research 27: 927-940.
25. Van Loosdrecht MCM, L. J., Norde W, Schraa G, Zehnder AJB (1987). "The role of bacterial cell wall hydrophobicity in adhesion." Applied and Environmental Microbiology 53(8): 1893-1897.
26. Wan A, W. R., Doherty PJ, Williams DF (1997). "A study of cell behaviour on the surfaces of multifilament materials." 45-51.
27. Briggs D., and Rance D.G. (1989). "Surface Properties," chapter in Comprehensive Polymer Science; Volume 2: Polymer Properties. Pergamon Press, New York.
28. Dekker A, r. K., Beugeling T, Bantjes A, Feijen J, van Aken WG (1991). "Adhesion of endothelial cells and adsorption of serum proteins on gas plasma-treated polytetrafluoroethylene." Biomaterials 12: 130-138.
29. Dadsetan M, M. H., Sharifi-Sanjani N, Daliri M (2001). "Cell behavior on laser surface-modified polyethylene terephthalate in vitro." Journal of Biomedical Materials Research 57: 183-189.
30. Lazare S, B. P. (1993). "Surface amorphization of Mylar films with excimer laser radiation above and below ablation threshold: ellipsometric measurements." Journal of Applied Physics 74(8): 4953-4957.
31. Krajnovich, D. (1997). "Near-threshold photoablation characteristics of polyimide and poly(ethylene terephthalate)." Journal of Applied Physics 82: 427-435.
32. Krajnovich, D. (1997). "Incubation and Photoablation of Poly(methyl methacrylate) at 248 nm. New insight into the reaction mechanism using photofragment translational spectroscopy." Journal of Physical Chemistry A 101: 2033-2039.
33. Dyer PE, K. D., Key PH, Tait JP (1996). "Excimer laser ablation of low and high absorption index polymers." Applied Surface Science 96-98: 596-600.

34. Kesting W, B. T., Schollmeyer E (1993). "The effect of vacuum-ultraviolet laser wavelengths on the surface treatment of polyolefinic polymers." Journal of Polymer Science B: Polymer Physics 31: 887-890.
35. Heszler P, K. L., Torok M (1991). "Model for the UV laser ablation of polymers in the low-fluence limit." Solid State Communications 78(5): 425-427.
36. Norton MG, J. W., Dickenson JT, Hipps KW (1996). "Pulsed laser ablation and deposition of fluorocarbon polymers." Applied Surface Science 96-98: 617-620.
37. Girardeaux C, I. Y., Pireaux JJ, Caudano R (1996). "Etching and functionalization of a fluorocarbon polymer by UV laser treatment." Applied Surface Science 96-98: 586-590.
38. Niino H, Y. A. (1996). "Chemical Surface modification of fluorocarbon polymers by excimer laser processing." Applied Surface Science 96-98: 550-557.
39. Laurens P, s. B., Decombert F, Arefi-Khonsari (1999). "Laser-induced surface modifications of poly(ether ether ketone): influence of the excimer laser wavelength." Journal of Adhesion Science and Technology 13(9): 983-987.
40. Yi X-S, F. Y. (1999). "Etching behavior of plastics using a near infared laser." Journal of Materials Science Letters 18(3): 245-247.
41. Song Q, N. A. (1999). "Effects of a pulsed XeCl excimer laser on ultra-high strength polyethylene fiber and its interface with epoxy resin." Journal of Adhesion Science and Technology 13(4): 501-516.
42. Viville P, B. S., Lambin G, Lazzaroni R, Bredas JL, Kolev K, Laude L (1996). "Excimer laser-induced surface modifications of biocompatible polymer blends." Applied Surface Science 96-98: 558-562.
43. Man HC, L. M., Yue TM (1998). "Surface treatment of thermoplastic composites with an excimer laser." International Journal of Adhesion and Adhesives 18: 151-157.
44. Srunivasan R, M.-B. V. (1982). "Self-developing photoetching of poly(ethylene terephthalate) films by far-ultraviolet excimer laser radiation." Applied Physics Letters 41(6): 576-577.
45. Sperling, L. (1992). Introduction to Physical Polymer Science. New York, John Wiley and Sons, Inc.

46. Lawrence J, L. L. (2001). "Modification of the wettability characteristics of polymethyl methacrylate (PMMA) by means of CO2, Nd:YAG, excimer and high power diode laser radiation." Materials Science and Engineering A303: 142-149.
47. "Standard Test Method for Tensile Properties of Plastics," 2001 ASTM standard Designation D 638-00, ASTM publishing; West Conshohocken, PA.
48. Lazare S, H. P., Baker JM, Srinivasan J (1984). Journal of the American Chemical Society 106: 4288.
49. Breuer J, Metev S, and Sepold G (1995). "Photolitic surface modification of polymers with UV-laser radiation." Journal of Adhesion Science and Technology 9(3): 351-363.
50. Brewis DM, Mathieson I, and Wolfensburger M (1995). "Treatment of low energy surfaces for adhesive bonding." International Journal of Adhesion and Adhesives 15(2): 87-91.
51. Brewis DM (1992). "Pretreatments of hydrocarbon and fluorocarbon polymers." Journal of Adhesion 37: 97-107.

9. Appendix

General materials characterization

Some other general materials characterization was carried out on each of the three samples to determine some of the basic material properties of the formulations used for this project. Differential Scanning Calorimetry was performed for determination of the glass transition temperature. Mechanical testing was performed and density measurements were also taken.

Using differential scanning calorimetry, thermal events such as the glass transition, melting, and crystallization temperatures can be determined from a plot of the differential heat flow versus temperature. An example plot of glycol-treated polyethylene terephthalate is shown in Figure 52 below.

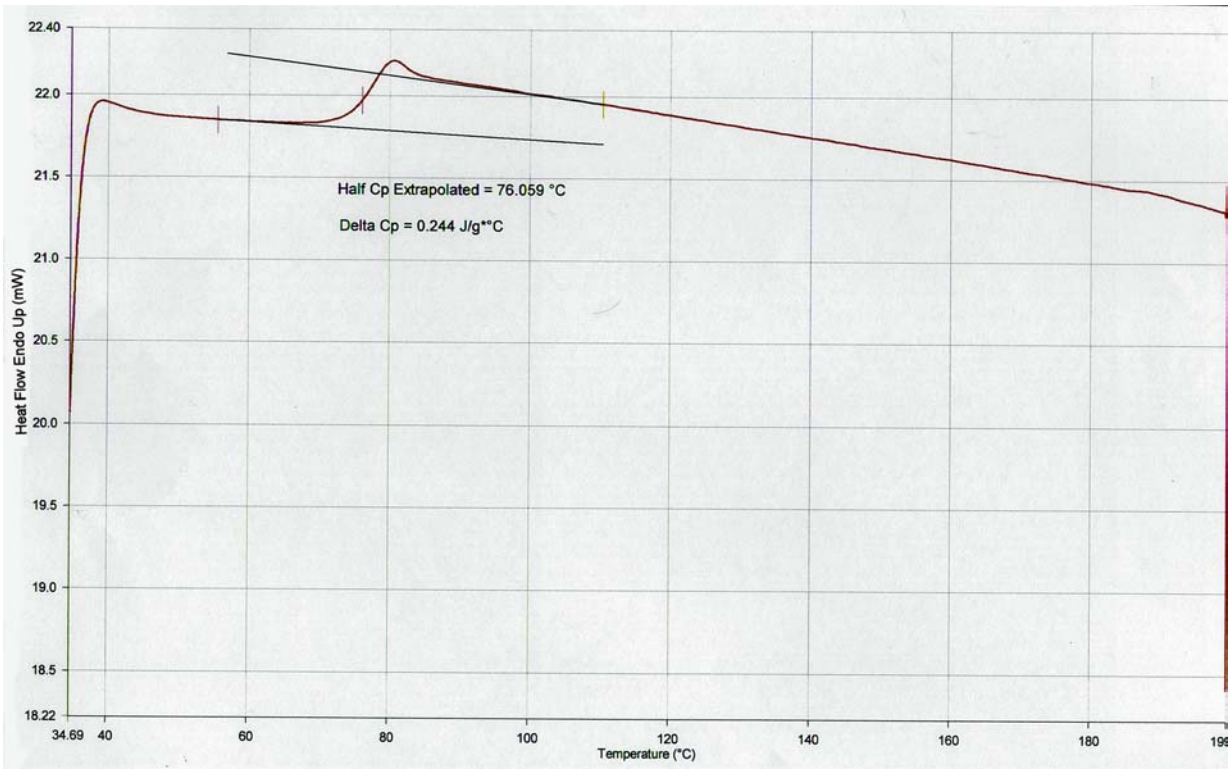

Figure 52- Sample DSC plot of heat flow versus temperature for glycol-treated poly(ethylene terephthalate)

The glass transition temperature is shown in such a plot as an endothermic shift during which one-half of the change in heat capacity has occurred [45]. The Pyris software used in this experiment contains a feature that calculates and displays the half-C_p temperature value. This value is taken to be the glass transition temperature.

DSC scans were run of each of the three materials. The experimental values for the glass transition temperatures along with published values are shown in Table 9.

Table 9 - Experimental and published glass transition temperatures for PETG, PMMA, and PTFE

Material	Experimental T_g Run 1 (°C)	Experimental T_g Run 2 (°C)	Experimental Average T_g (°C)	Published T_g value (°C)
PETG	76.059	74.472	75.266	
PMMA	104.948	104.782	104.865	105 [45]
PTFE	49.268	49.419	49.344	-113 [45]

Mechanical testing was performed using dog bone specimens consistent with the standards described in ASTM D 638-00 Standard Test Method for Tensile Properties of Plastics [47] and a Texture Analyzer test frame with tensile grips. Eight specimens per material were tested in tension to failure. The results of the mechanical testing are shown in Figure 53 and 54.

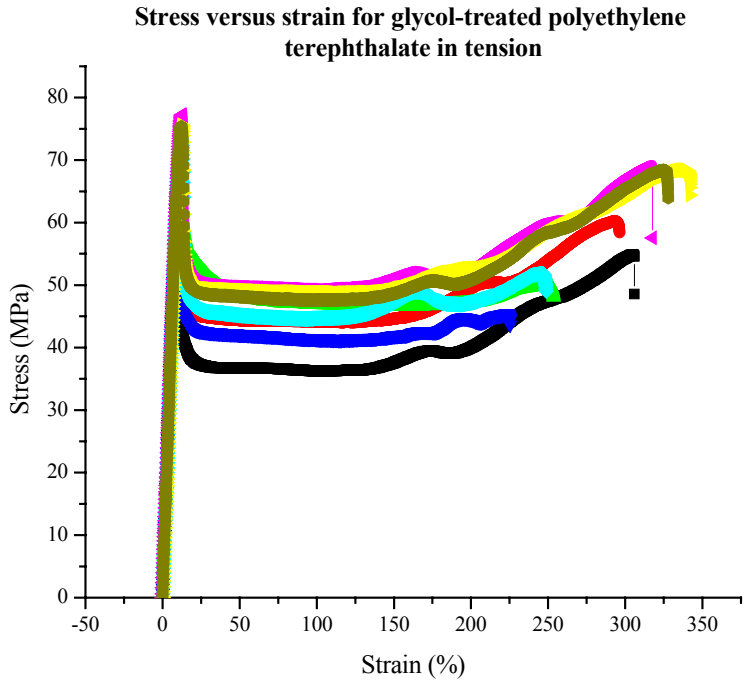

Figure 53 - Stress versus strain for PETG in tension

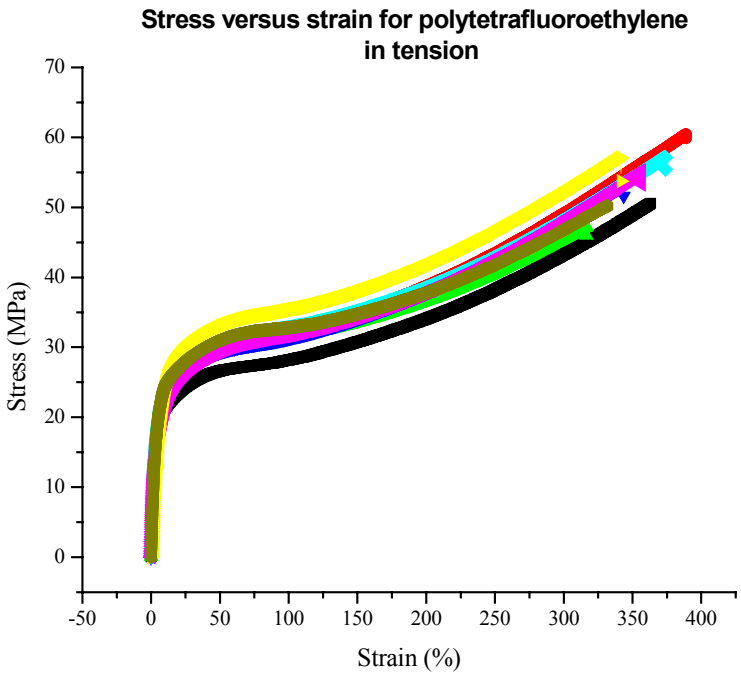

Figure 54 - Stress versus strain for PTFE in tension

From the stress versus strain plots for the three materials, the elastic modulus was calculated from the slope of the curve in the region of elastic deformation. The results of these calculations are shown Table 10.

Table 10 - Modulus calculations from tensile strength testing of PETG and PTFE

Sample	PETG - E (MPa)	PTFE - E (MPa)
1	683.06	490.05
2	670.25	461.14
3	676.86	401.63
4	665.42	455.28
5	667.88	436.19
6	631.65	472.85
7	651.86	403.29
8	636.47	425.87
Average Modulus (MPa)	660.43	443.29
Standard Deviation (MPa)	18.65	32.10

8. Vita

Allison Elizabeth Suggs was born on April 30, 1978 in Eugene, Oregon to Dr. William W. Suggs and Mary Claire Suggs. She graduated from Patrick Henry High School in Roanoke, Virginia in June of 1996 after which she began studies towards her bachelor's degree in the Materials Science and Engineering Department at Virginia Tech. During her undergraduate career, Allison worked in the polymer laboratory for Dr. Brian Love doing undergraduate research in the areas of polymers, biomaterials, and adhesives. Upon graduation in May 2000, Allison took an internship at Intel Corporation in Portland, Oregon after which, she returned to Virginia Tech where she pursued her M.S. also in materials science. Allison is now working in Fairfax, Virginia for Materials Modification Incorporated doing research and development in the areas of polymers and nanomaterials.